INL/EXT-13-28293

Rapid Analysis of Ash Composition Using Laser-Induced Breakdown Spectroscopy (LIBS)

Tyler L. Westover

January 2013

The INL is a U.S. Department of Energy National Laboratory
operated by Battelle Energy Alliance

INL/EXT-13-28293

Rapid Analysis of Ash Composition Using Laser-Induced Breakdown Spectroscopy (LIBS)

Tyler L. Westover

January 2013

Idaho National Laboratory
Biofuels and Renewable Energy Technologies Division
Idaho Falls, Idaho 83415

http://www.inl.gov

Prepared for the
U.S. Department of Energy
Assistant Secretary for Energy Efficiency and Renewable Energy
Under DOE Idaho Operations Office
Contract DE-AC07-05ID14517

ABSTRACT

Inorganic compounds are known to be problematic in the thermochemical conversion of biomass to syngas and ultimately hydrocarbon fuels. The elements Si, K, Ca, Na, S, P, Cl, Mg, Fe, and Al are particularly problematic and are known to influence reaction pathways, contribute to fouling and corrosion, poison catalysts, and impact waste streams. Substantial quantities of inorganic species can be entrained in the bark of trees during harvest operations. Herbaceous feedstocks often have even greater quantities of inorganic constituents, which can account for as much as one-fifth of the total dry matter.

Current methodologies to measure the concentrations of these elements, such as inductively coupled plasma-optical emission spectrometry/mass spectrometry (ICP-OES/MS) are expensive in time and reagents. This study demonstrates that a new methodology employing laser-induced breakdown spectroscopy (LIBS) can rapidly and accurately analyze the inorganic constituents in a wide range of biomass materials, including both woody and herbaceous examples. This technique requires little or no sample preparation, does not consume any reagents, and the analytical data is available immediately. In addition to comparing LIBS data with the results from ICP-OES methods, this work also includes discussions of sample preparation techniques, calibration curves for interpreting LIBS spectra, minimum detection limits, and the use of internal standards and standard reference materials.

SUMMARY

The results from the LIBS calibrations for Al, Ca, Fe, Mg, Mn, P, K, Na and Si is presented in Table 1 and Figures 8 through 11 and indicate that LIBS is promising as a rapid screening technique with an accuracy comparable to that of the acid digestion methods for all of the elements. Importantly, ICP-OES/MS methods, which involve acid digestions, have benefited from many years of widespread research and repeated use, while the LIBS approach is yet emerging for measuring inorganic constituents in biomass. Accordingly, significant improvement is expected in the LIBS approach. For example, the LIBS calibrations in this work employ univariate curve fits, which are usually quite poor compared multivariate calibrations, although the simplicity of univariate methods makes them attractive. A further consideration is that the univariate LIBS calibrations exhibit a high degree of correlation, considering uncertainties in calibration data, and it is possible that multivariate models would only improve the fits by modeling experimental noise, which could make the fits less reliable for new samples. Multivariate models do have advantages, though, in being able to account for interaction effects between elements of interest. It is demonstrated in Fig. 12 that LIBS is useful for measuring total ash content minus, except Cl and S. Further refinement to the LIBS technique, such as a more sensitive detector or the use of an argon purge gas should make it possible to reliably analyze Cl, S and possibly O, N, and H.

It is observed that the LIBS calibration curves for some elements for non-NIST samples follow different trends than the corresponding fits for the NIST SRMs. The reason for this discrepancy is not clear. All of the samples were ground to similar fine particles sizes (minus 80 microns) and were subjected to a similar pelletization procedure. The LIBS measurements were randomized with some repeated points, and it was verified that equipment drift over the time duration of the experiments was not a significant factor. It is also unlikely that the calibration data for the non-NIST samples are in error because similar results were obtained using three separate methods and instruments at different laboratories. Regardless of the reason for the discrepancy, assuming that the calibration data is accurate, the LIBS calibration curves for the non-NIST samples are valid. Perhaps the cause of the discrepancy between the NIST SRMs and the non-NIST samples will become clearer as additional samples are tested and validated with independent ICP-OES methods.

ACKNOWLEDGEMENTS

Byron White conducted the ICP-OES analyses of the inorganic composition of the samples at INL. Also, several interns assisted in preparing samples and collecting data using the LIBS instrument. They are Justin Dayley (Brigham Young University-Idaho), John Dalton (Brigham Young University-Idaho), Samuel Goodrich (Brigham Young University-Idaho), Braden Haws (Brigham Young University-Idaho), and Trevor Terrill (Brigham Young University-Idaho).

Rapid Analysis of Ash Composition Using Laser-Induced Breakdown Spectroscopy (LIBS)

1. OBJECTIVE AND EXPECTED OUTCOME

The goal of the biofuel's feedstock supply system is to deliver uniform, quality-assured feedstock materials that will enhance downstream system performance by avoiding problems in the conversion equipment. Rapid screening of carbohydrate data is provided by near-infrared and mid-infrared spectrometries. However, rapid screening techniques do not exist to analyze inorganic elements in biomass that create a number of downstream problems in thermochemical processes. The primary problematic inorganic constituents are Si, K, Ca, Na, S, P, Cl, Mg, Fe and Al. In particular, these elements reduce the energy content of the feedstock, influence reaction pathways, contribute to fouling and corrosion within systems, poison catalysts, and impact waste streams.

Laser-induced breakdown spectroscopy (LIBS) has been identified as potential technique that could allow rapid elemental analyses of the inorganic content of biomass feedstocks because it incorporates the following features/benefits:

- Performs rapid, in situ, multi-element analysis
- Requires little or no sample preparation, although grinding & pelletization is helpful
- Minimizes sample contamination risks
- Produces no waste streams
- Allows high spatial resolution measurement in small sample volumes
- Non- or minimally-destructive
- Can be designed as user-friendly, field-portable system.

The mineral content and composition is recognized as both a barrier to the use of some feedstocks and as a quality attribute that may be controlled through the feedstock assembly process. The inorganic content of biomass feedstocks is known to vary over wide ranges, depending upon the plant type and anatomical fraction, growing conditions, harvesting time and method, and handling operations. The expected outcome of this task is to develop a LIBS tool that is capable of reliably analyzing a wide range of inorganic elements in biomass from a concentration range as low as a few parts per million (ppm) to as high as a few percent. Analyses using a LIBS tool will require little if any sample preparation, will produce no waste stream, and will provide immediate characterization data. Development of a cost-effective screening tool will open opportunities to rapidly analyze inorganic constituents in biomass to facilitate quickly blending diverse feedstocks to produce on-spec materials that will in turn, reduce the capital and maintenance of operating costs of thermochemical conversion platforms.

2. INTRODUCTION

Ash, the noncombustible constituents in biomass, is known to contribute to several problems in conversion processes, such as fouling of reactor surfaces and influencing reaction pathways to reduce of yields and increase waste streams. The ash content in biomass is known to vary over a wide range and is influenced by plant type, growing conditions, harvesting methods, and handling operations. If the mineral content can be readily and inexpensively obtained, mixing of diverse biomass materials can yield

feedstocks that minimize the associated problems with ash, thereby reducing maintenance, replacement, and cleaning cost to capital equipment.

The current methods for determining ash content in biomass include inductively coupled plasma-optical emission spectrometry, ICP-OES (Aarujo et al., 2002; Momen et at., 2006), inductively coupled plasma-mass spectrometry, ICP-MS (Alvarado et al., 1996), and flame atomic absorption spectrometry, FAAS (Baker and Grewelin, 1967). These methods in general require significant sample preparation, consuming both reagents and time. Laser induced breakdown spectroscopy (LIBS) is currently being investigated as a method to rapidly screen and determine the mineral concentration of a wide variety of biomass. LIBS requires little sample preparation and can provide immediate results upon testing. It is a potential low-cost alternative that will allow rapid screening of biomass feedstocks.

In LIBS, a small sample of material is ablated with a high-energy pulsed laser. The impact of the laser pulse with the sample surface immediately results in a short-lived strong continuum emission due to the collision between free electrons and the excited atoms and ions. As the plasma expands and cools, the continuum radiation rapidly decays. Since the atoms of different elements have a number of different energy states with different transition probabilities, a number of spectral peaks are produced. The sensitivity of a peak depends upon the probability of an electron making a particular transition that produces light at that wavelength, and since some transitions are more probable than others with more energy levels available to them, some peaks are more intense and have different life times than others. Emitted light from the sample is focused onto a spectrometer and analyzed by an intensified charge couple device. Since elements have unique excitation energies, emitted light from each element and its ions contains unique spectral data about that element. These spectral lines can be quantitatively analyzed to determine concentrations of the corresponding element by comparing the intensity of elemental spectral peaks with the known concentration of the sample. Important parameters in optimization the LIBS signal for particular elemental and ionic peaks include the gate delay time between the firing of the laser and opening of the shutter of the spectrometer, the time that the spectrometer acquires emitted light (gate width), and the laser spot size, power and pulse time duration. All elements at sufficiently high temperatures emit light of characteristic frequencies. Consequently, in principle, it is possible to analyze any element in a sample by this method.

In recent years, attention has been turned to using LIBS for a quantitative analysis of the mineral composition in biomass. Due to the flexibility of LIBS, both macronutrients (N, P, K, Ca, Mg and S) and micronutrients (Fe, Cu, Mn, Zn, B, Mo, Ni and Cl) can potentially be analyzed with this technique. Sun et al. (Sun et al., 1999) used NIST certified reference materials and mixtures of these materials to construct LIBS calibration curves, which were employed with LIBS analysis to determine the concentration of Ca, Mg, P, Fe, Cu, Mn, Zn, and Al in plant leaves. It was found that a gate delay of 1 μs and an integration time of 10 μs provided the optimum signal to noise ratio and that the coefficient of variation of measurements was approximately 8-15%. Gornushkin el al. investigated the influence of the matrix on Mg signals in powdered samples, and proposed a surface density normalization method to compensate matrix effects that are problematic for quantitative elemental analysis. Gornushkin et al. noted that the Mg II weak lines at 292.78 and 283.65 nm were observable and could be used for quantitative analysis at concentrations above 0.7%. For samples with very low concentrations (even below 0.001%), the strong ionic lines at 279.806 and 280.27 nm and the atomic line at 285.213 nm can be used. However, these strong lines experience substantial self-absorption at concentrations approaching 0.5%, which limits their range of linear dynamic response.

More recently, Nunes et al. optimized LIBS parameters and validated the LIBS approach for the determination of macronutrients P, K, Ca, and Mg and micronutrients B, Cu, Fe, Mn, and Zn in pelletized sugar cane leaves. Quantitative determinations were performed using univariate calibration and chemometric methods on a total of 26 laboratory reference samples to construct calibration curves and an additional 15 test samples to validate the method. The samples were also microwave-assisted digested and

analyzed by ICP OES for comparison. Repeatability precision of measurements obtained by univariate and multivariate calibrations ranged from 1.3 to 29% and 0.7 to 15%, respectively, demonstrating that LIBS is a powerful tool for analysis of plant pelletized material. Additional studies have shown calibration curves can be constructed for certified reference materials using both univariate and multivariate approaches (Labbe et al., 2008; Braga et al., 2010).

The principal challenge in LIBS as a potential feedstock screening technique lies in poor correlation of certain measured LIBS intensity values with analytical concentration values in several elements. These are manifest as apparent outliers or spread in the data outside of tolerance limits. There are several potential causes for the presence of these discrepancies, including the inability of LIBS to measure mineral composition of widely varying materials with a single calibration curve; interactions between elements in the plasma plume that influence LIBS intensity data; and possible errant analytical concentration data used to build the calibration curve. The cause of these outliers needs to be determined and mitigated before LIBS can be employed to reliably analyze inorganic constituents in biomass feedstock materials.

The purpose of this work is to develop LIBS calibration curves for multiple elements, including Al, Ca, Fe, K, Mg, Mn, Na, P and Si that can be applied to a wide variety of biomass materials for measuring ash composition. Twelve different biomass samples of widely varied ash composition have been used build the LIBS calibration curves. Six of the materials are Standard Reference Materials (SRMs) from the National Institute of Standards and Technology (NIST). The inorganic constituents in these materials have been analyzed, and NIST has published certified concentrations for many of the inorganics. Six other biomass materials were also chosen, and the mineral concentration of these additional biomass samples was determined by independent ICP-OES analysis. LIBS calibration curves were developed by comparing LIBS results from element concentration values obtained from NIST and independent ICP-OES methods.

3. METHODS

3.1 Sample preparation

Samples from 12 different types of biomass were used for the evaluation of LIBS. Six of the samples were NIST certified reference materials (SRMs), which have been ground to minus 75 microns and have guaranteed inorganic concentration values. The following six NIST samples were used for calibration: apple leaves NIST 1515 (ApLe), peach leaves NIST 1547 (PeLe), spinach leaves NIST 1570a (SpLe), tomato leaves NIST 1573a (ToLe), pine needles NIST 1575a (PiNe), and wheat flour NIST 1567a (WhFl). The other six samples, which are common materials of interest as biofuel's feedstocks, include the following: corn stover (CnSt), miscanthus (Misc), reed canary grass (ReCG), sorghum (Sorg), switchgrasss (SwGr), and wheat straw (WhSt). The samples were prepared by grinding them to minus 80 microns. Pellets were made for LIBS analysis from the remaining split sample by placing approximately 1 gram of sample powder in a 0.5 inch diameter pellet die and applying approximately 100 ksi of pressure for one minute. For an internal standard validation, germanium powder (particle size less than 50 microns) was added to the biomass at known concentrations of 20,000 ppm (2% by mass) after the biomass was ground. The biomass with the germanium powder was thoroughly mixed following the method published by NIST on the SRM certificates and then pelletized following the procedure described above.

3.2 Independent ash composition analysis by ICP-OES

After being ground to minus 80 microns, three methods were employed to prepare the samples for ICP-OES or ICP-MS analysis. The first method was applied at Idaho National Laboratory by digesting the sample powders in closed beakers using a microwave assisted process in hydrofluoric (HF) acid. The

second and third methods were both employed at Huffman Laboratories, Inc. (Golden, CO). In the second method, the samples were digested in duplicate with nitric (HNO3) and refluxing perchloric (HClO4) acids to fully oxidize all organic material present. In the third method, the samples were first staged by ashing 750°C for 8 hours and then subjected to a lithium metaborate fusion process. In the remainder of this report, these three methods are referred as the 'HF acid' method, the '2 acid' method, and the 'LMF' method, respectively.

3.3 LIBS Experimental Parameters

A modified RT-100 (Applied Spectra, Inc., Fremont, CA) was used to perform the LIBS measurements. In this instrument, laser excitation was provided by a pulsed Nd:YAG laser with a wavelength of 1064 nm and a 7 ns pulse in air. The laser was capable of a maximum of 90 mJ per pulse and was operated at 80% of maximum. The laser focusing lens had a focal length of 15 mm. A 5-channel spectrometer system with approximately 1.5 nm resolution was used with a charge couple device (CCD). Samples were tested with gate delay times of 1 and 3 μs and a gate width of 1 ms.

LIBS spectra were collected at 40 different sample sites, 20 sites on each side of the pellet. Each sample site consisted of 20 consecutive laser pulses on the surface for improved precision. The gate width (GW) for the collection of the LIBS signal by the spectrometer was 1.0 ms for all presented experimental results. The laser was focused 0.3 mm below the sample surface (Z_{Focus} = -0.3 mm). Multiple replicates of each sample were tested to ensure repeatability and precision of results.

3.4 Univariate calibration for inorganic constituents

Many elements exhibit signature peaks multiple wavelengths, so the entire wavelength range from 200 nm to 1000 nm was searched to identify every peak possible for each element of interest. Each peak in the collected spectra was identified based on NIST and other spectroscopic databases. In some cases, peaks from different elements can overlap in the same wavelength region causing interference and making it difficult to determine the concentrations of particular elements using only a single peak for each element. To avoid such difficulties and to ensure that the LIBS calibrations models are as robust as possible, multiple peaks were identified for each element. In the cases that multiple peaks yield similar predictions for the concentration of a particular element, the confidence in the prediction increases. Multiple spectral peaks for each element were evaluated for use in the calibration curve according to signal-to-noise ratios, strength of spectral peaks, and interferences from adjacent peaks. Spectral peaks were chosen to optimize linear correlations between spectral peak intensity values and measured concentration values.

Spectral data were imported into Microsoft Excel for data processing. The background noise level was determined by fitting a straight line through several data points on each side of each spectral peak of interest, and care was taken to ensure that the intervals selected for background determination did not contain any visible peaks. After the background noise was determined, it was subtracted from the peak of interest. Peak intensities were measured by the area under the spectral peak after background correction. For the NIST samples, measured LIBS peak intensities were plotted as a function of concentration certified by NIST, and calibration curves were calculated following the development described by Draper and Smith (Draper and Smith, 1998). The magnitudes of the fit residuals suggested that the errors between the best fit lines and measured LIBS intensities increased somewhat with LIBS intensity but did not follow Poisson statistics in which the uncertainty in measured signal intensity is proportional to its own square root (Bevington and Robinson, 2003). Consequently, it was assumed that uncertainties in the LIBS measurements were approximately constant (i.e. independent of the magnitude of the measured LIBS intensity). Assuming that the measurement uncertainty was constant, 95% confidence intervals were also calculated for predicting elemental concentrations from measured LIBS values.

3.5 Peak normalization

In addition to building calibration curves based on the measured intensities of all identified LIBS peaks, the measured intensities were also normalized using the measured intensities of the hydrogen peak at 656 nm, the carbon peaks at 248 nm and 909 nm, as well as germanium peaks at 265 nm and 304 nm for samples that had been doped with germanium. Normalization by the carbon peak at 248 nm (C 248 nm) and the germanium peak at 265 nm (Ge 265 nm) exhibited the best fit performance, so only those results are shown below

4. RESULTS AND DISCUSSION

4.1 Assessment of inorganic analysis methods using NIST Standard Reference Materials (SRMs)

The three ICP-OES/MS methods described above were applied to six NIST standard reference materials (SRMs) in order to compare the reliability and accuracy of the methods. The results for calcium, magnesium, potassium, and sodium are shown in Figure 1. Due to limitations, not all analyses were available for all of the elements using all of the methods. For all four elements, all three methods yielded results that are in reasonable agreement with the NIST values, although there are a few notable exceptions. Of particular concern are the reported values of magnesium in tomato leaves and sodium in peach leaves and apple leaves. In these examples, two of the test methods yielded values that were significantly different than the NIST certified values, although they were in reasonably close agreement with each other. Cases in which two independent methods yield similar results that are both in error are difficult to diagnose in building calibration curves.

Figure 2 displays similar data for aluminum, iron, manganese, and phosphorus. Again, for all of these elements, all three ICP-OES methods yielded concentration values in reasonable agreement with the NIST certified values with few exceptions.

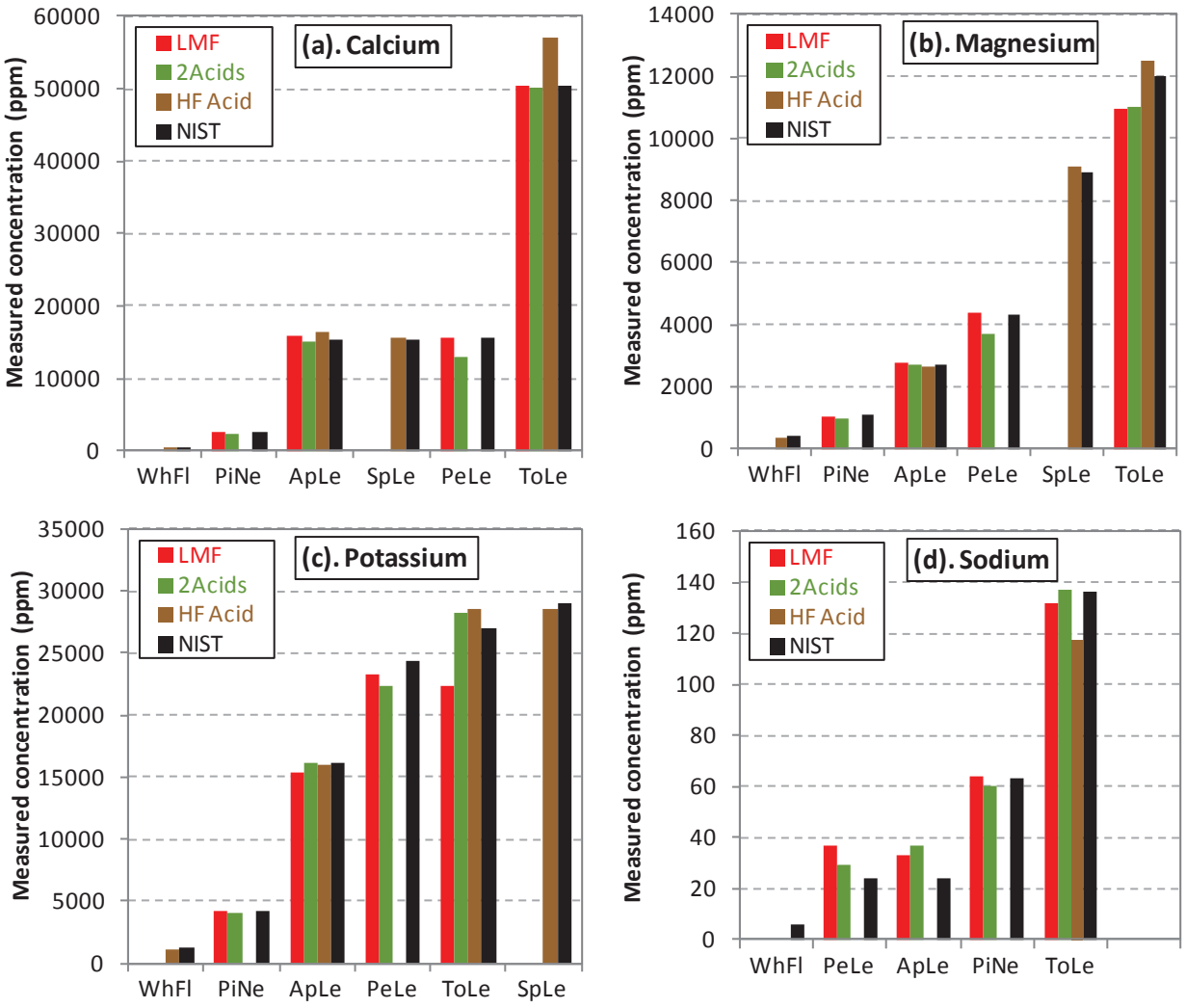

Figure 1. Measured concentrations of Ca, Mg, K, and Na for six NIST SRMs as determined using ICP-OES methods with HF acid digestion, HNO3 and HClO4 acid digestions (labeled '2 Acids'), and a lithium metaborate fusion (LMF) method.

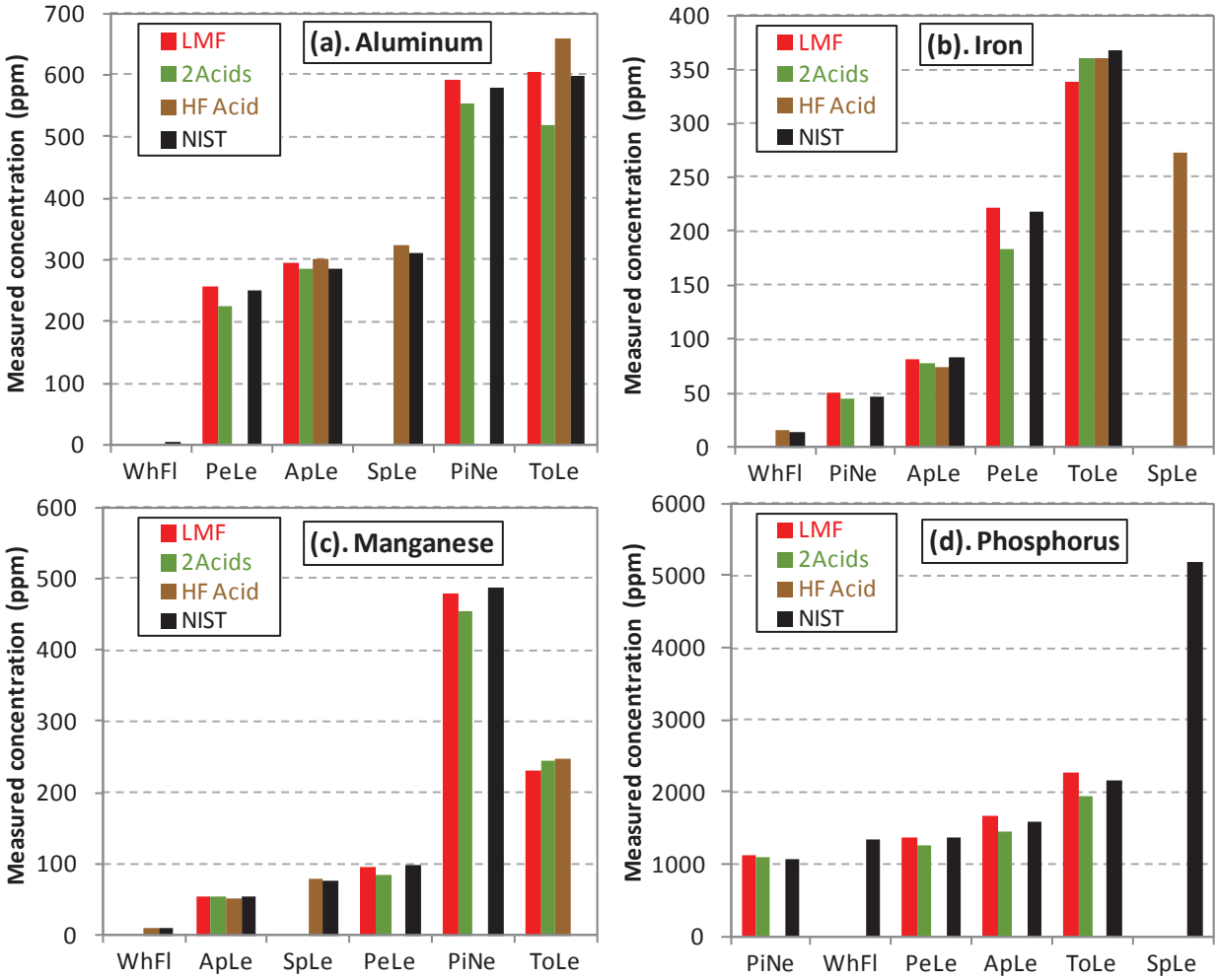

Figure 2. Measured concentrations of Al, Fe, Mn, and P for six NIST SRMs as determined using ICP-OES methods with HF acid digestion, HNO3 and HClO4 acid digestions (labeled '2 Acids'), and a lithium metaborate fusion (LMF) method.

4.2 Analysis of inorganic species in non-NIST samples

Biomass feedstock materials may differ substantially from NIST SRMs. Consequently, it is necessary to include a wide variety of potential feedstock materials in LIBS calibration models. However, accurately determining the inorganic constituents in these materials can be challenging. The three ICP-OES/MS methods described above were applied to six non-NIST biomass materials, including corn stover (CnSt), miscanthus (Misc), reed canary grass (ReCG), sorghum (Sorg), switchgrass (SwGr), and wheat straw (WhSt) in order to reliably establish the concentrations of the inorganic constituents in these materials. The results for calcium (Ca), magnesium (Mg), potassium (Mg), and sodium (Na) are shown in Figure 3. For Ca, Mg, and K, the results from the different methods are in good agreement for nearly all samples. For sodium, there are several discrepancies. For most samples, results from at least two of the methods exhibited good agreement which was often different from that of the third method. In such cases, the best estimated elemental concentration was calculated as the mean of the two results in closest agreement. The best estimated concentrations of Ca, Mg, K, and Na calculated in this way for each of the samples is shown in Fig. 3 as black bars.

Figure 4 displays the results of the three ICP-OES/MS methods described above to analyze aluminum (Al), iron (Fe), manganese (Mn), phosphorus (P), and silicon (Si) in the six non-NIST biomass materials. For Al, the '2 acid' method exhibited results that were significantly different than that of the other two methods for all samples. For the other elements, the results from the different methods were in fairly good agreement. Note, that due to limitations, not all methods could be employed to analyze all elements. Figure 4f presents the measured Si concentrations for the six NIST SRMs (certified values for Si are not available from NIST for these SRMs). As was the case for Fig. 3, the best estimated concentration of each element in each sample (black bars) was calculated from the mean of results that were in the closest agreement.

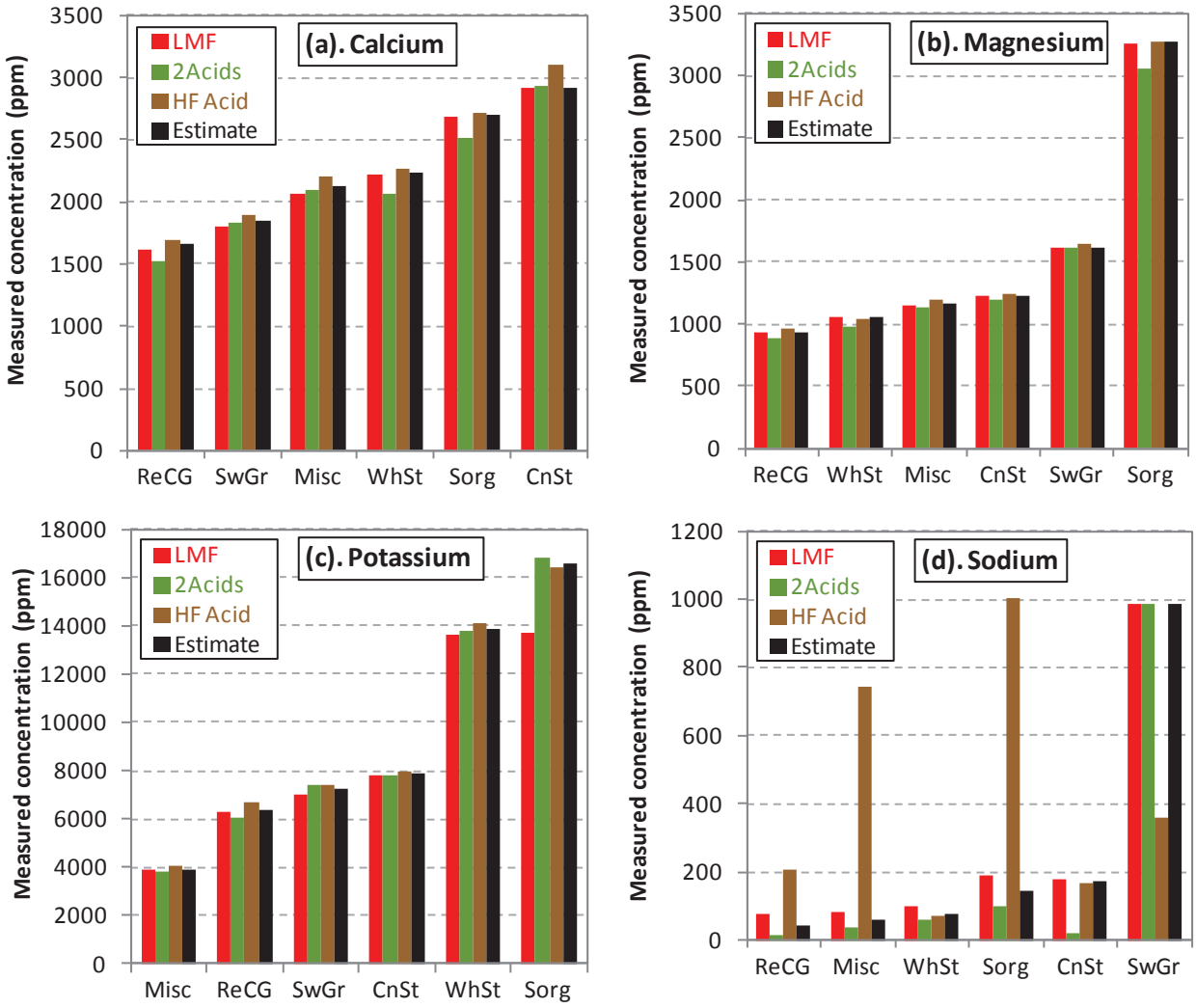

Figure 3. Measured concentrations calcium (a), magnesium (b), potassium (c), and sodium (d) for six non-NIST samples as determined using ICP-OES methods with HF acid digestion, HNO3 and HClO4 acid digestions (labeled '2 Acids'), and a lithium metaborate fusion (LMF) method.

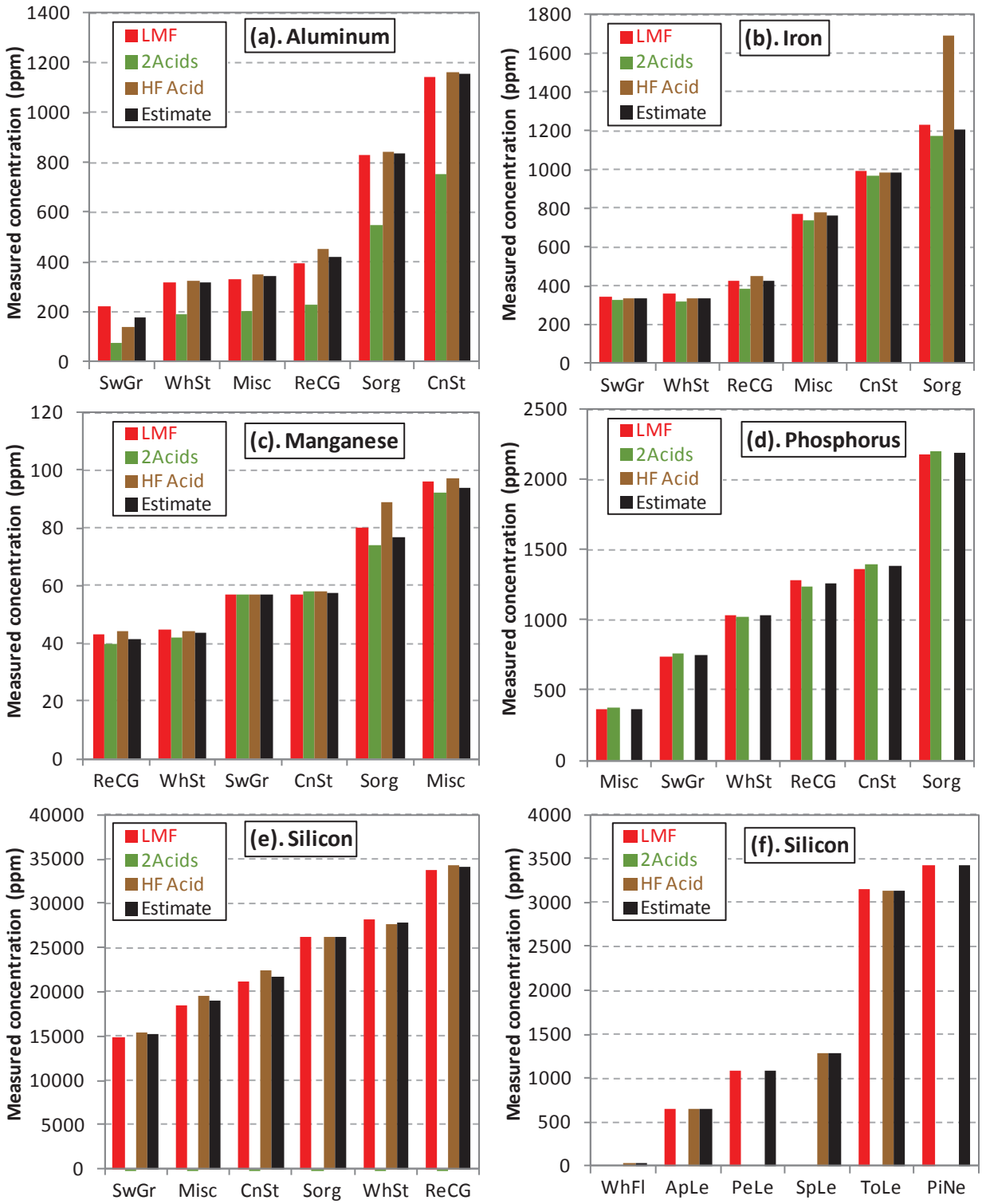

Figure 4. Measured concentrations aluminum (a), iron (b), manganese (c), phosphorus (d) and silicon (e) for six non-NIST samples as determined using ICP-OES methods with HF acid digestion, HNO3 and HClO4 acid digestions (labeled '2 Acids'), and a lithium metaborate fusion (LMF) method. Due to limitations, not all methods could be employed to analyze all elements. (f) contains similar Si concentration data for the NIST SRMs.

4.3 Validation of germanium as a potential internal standard

Figure 5a contains LIBS spectra near the Ge 265 nm peak from NIST 1515 apple leaves and NIST 1575 pine needles mixed with as much as 4% Ge powder by weight. Importantly, the area under each curve increases with Ge concentration, and the fact that the peaks obtained from the apple leaves and from the pine needles are approximately the same size for similar levels of Ge concentration indicates that both of these materials respond to the laser excitation approximately the same (i.e. both samples exhibit nearly the same matrix effects). The areas under the LIBS peaks in Fig. 5a were calculated are plotted in Fig 5b as functions of known Ge concentration. The results from a similar calculation for the areas under the Ge 303 nm peak are also shown and demonstrate that the relationship between the LIBS response and Ge concentration is approximately linear, especially for Ge concentrations less than 2%. The linearity of the LIBS signal with Ge concentration is crucial in making it possible to use Ge as an internal standard to validate the LIBS measurements.

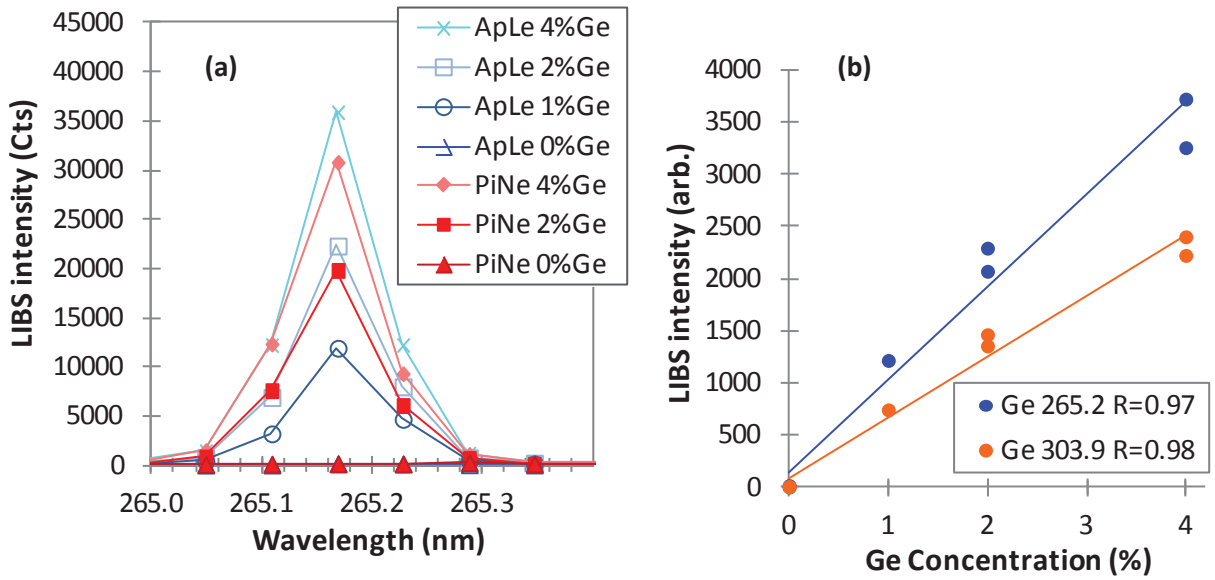

Figure 5. LIBS data from NIST 1515 apple leaves and NIST 1575 pine needles mixed with up to 4% Ge powder. (a) LIB spectra near the Ge 265 nm peak. (b) Calculated areas under the Ge 265.2 nm peak in (a) and the Ge 303.9 nm peak as functions of known Ge concentration. Gate delay (GD) = 2.0 μs for all spectra.

4.4 LIBS analysis of NIST SRMs and non-NIST samples

As described above, the gate delay time between the firing of the laser and opening of the shutter of the spectrometer greatly affects LIBS detection sensitivity. Spectra was collected using gate delay (GD) times of 1 and 3 μs to determine the optimal gate delay time for each element of interest. Table 1 summarizes the LIBS peaks that were found most helpful for obtaining calibration curves to analyze inorganic species in the samples tested in this work. Results are presented for the optimal GD and spectra normalization method (none, normalization by the C 248 nm peak or normalization by the Ge 265 nm peak) for each elemental peak of interest. Separate fits were created for the NIST SRMs and the non-NIST samples because in many instances the non-NIST samples exhibited calibration trends that were different from those of the NIST SRMs for many of the peaks. The calibration curves that were developed for the various elements of interest for the NIST SRMs and the non-NIST samples are described below. Note that the coefficient of determination (R^2) for nearly all of the fits is greater than 0.95, which is remarkable considering the uncertainty in the calibration data that is manifest in Figures 1-4. The LIBS

calibration fits that were developed for the various elements are presented and discussed in the following paragraphs.

The areas under the Mg peak at 278.5 nm for all of the NIST and non-NIST samples are plotted in Fig. 6a as a function of Mg concentration for a gate delay (GD) of 1 µs. NIST SRMs that have certified concentration values are shown as solid circles, while the non-NIST samples are shown as hollow circles. The thick solid line is the best fit line for the Mg 278.5 nm peak based on the NIST SRMs (solid dots), and the blue thin lines show the associated 95% confidence interval for predicting Mg concentration for a future NIST SRM. Estimated Mg concentrations for the non-NIST sample were obtained from the estimated values in Fig. 3. The NIST and non-NIST samples appear to follow similar trends and could be fit with a single calibration curve. The best fit for the Mg 278.5 nm peak based on the non-NIST samples is shown as a thick dashed line. The thin dashed lines show the associated 95% confidence interval for predicting Mg concentration for a future non-NIST sample. Note that the 95% confidence interval for the non-NIST samples is smaller than that of the NIST SRMs, primarily because the range of magnesium concentrations is much smaller for the non-NIST samples.

Table 1. LIBS spectral peaks that were found most useful for building LIBS calibration curves. The optimal gate time (GD) for each peak and the LIBS calibration curve parameters, including curve sensitivity (slope, b), coefficient of determination (R^2) and 95% prediction uncertainty (standard error, $U_{95\%}$). Results are listed separately for the NIST SRMs and non-NIST samples.

		NIST SRMs					non-NIST samples				
Species	Peak position (nm)	GD (us)	Norm.	b (cts/ppm)	R^2	$U_{95\%}$ (ppm)	GD (us)	Norm.	b (cts/ppm)	R^2	$U_{95\%}$ (ppm)
Al I	394.5	3	C248	0.57	0.97	45	1	None	0.66	0.98	51
Al I	308.3	3	None	4.93	0.98	37	3	None	3.22	0.98	49
Ca II	370.6	3	C248	0.09	1.00	809	1	C248	0.05	0.96	93
Ca II	849.8	3	C248	0.31	1.00	691	1	Ge265	0.07	0.90	144
Ca II	315.9	3	C248	0.14	0.99	1098	1	C248	0.08	0.90	150
Fe I	438.3	1	Ge265	1.33	1.00	8	1	None	2.6	0.99	44
Fe II	259.9	1	None	6.19	0.98	18	1	None	16	0.96	83
Fe II	261.2	1	None	0.45	0.97	24	1	None	0.90	0.99	46
K I	766.5	3	None	7.9	0.98	1488	1	None	8.0	0.96	912
K I	693.9	3	None	0.28	0.92	3034	3	None	0.27	0.93	1088
K I	404.5	1	Ge265	0.07	0.94	2525	3	None	0.06	0.76	1954
Mg I	518.3	3	None	0.29	0.99	277	1	Ge265	0.17	0.99	83
Mg II	278.5	3	None	0.01	0.99	335	1	Ge265	0.03	0.91	234
Mg I	309.1	3	None	14.8	1.00	233	1	Ge265	7.9	1.00	51
Mn II	257.6	1	Ge265	2.94	1.00	7	1	Ge265	7.9	0.80	9
Mn I	403.2	1	Ge265	7.9	1.00	7	1	Ge265	17	0.74	10
Na I	589	1	Ge265	1198	0.91	13	1	None	392	0.97	60
Na I	819.5	1	C248	16	0.81	17	3	None	2.25	0.96	68
P I	213.6	1	C248	0.03	0.99	170	1	Ge265	0.03	0.92	162
P I	255.3	1	C248	0.03	0.96	287	1	Ge265	0.02	0.94	139
Si I	251.6	1	None	0.59	0.75	604	3	C248	0.29	0.98	1702
Si I	243.6	1	None	0.02	0.80	544	3	C248	0.01	0.99	1268
Si I	288.2	1	None	0.21	0.87	441	3	C248	0.12	0.98	1368

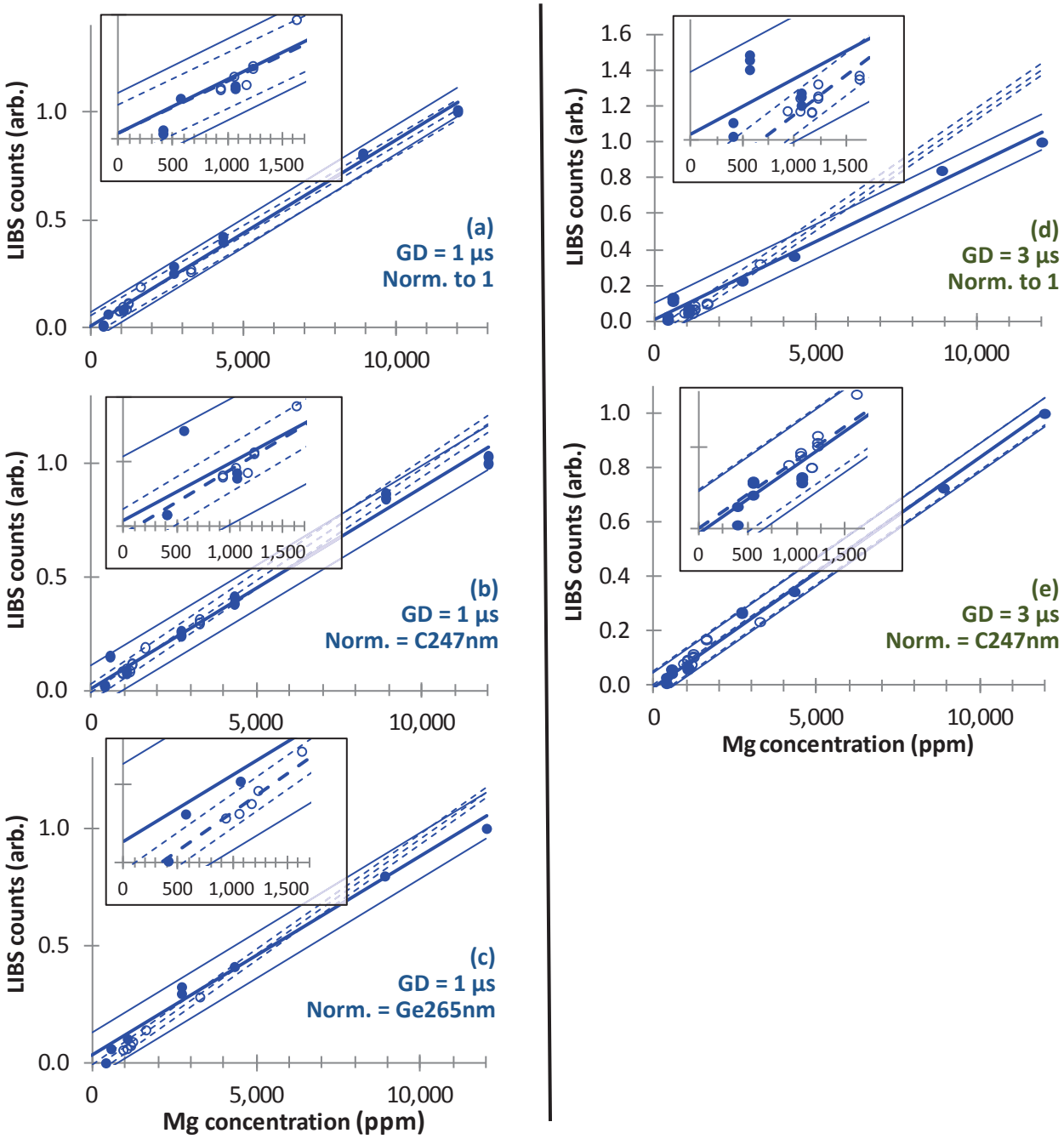

Figure 6. LIBS calibration data for magnesium using the Mg 278.5 nm peak. The area under the peak is plotted as a function estimated Mg concentration for all NIST (solid dots) and non-NIST samples (hollow circles). Estimated Mg concentration data was obtained for the NIST and non-NIST samples from Figures 1 and 3, respectively. In (a), the gate delay (GD) was 1 µs and the curves were normalized to have a maximum of unity. Plots (b) and (c) are similar to (a) except that the areas under the Mg 278.5 nm peak has been normalized by the carbon peak at 247.8 nm and the germanium peak at 265.1 nm, respectively. (d) and (e) are similar to (a) and (b), respectively, except that GD = 3 µs.

Figures 6b and 6c are similar to 6a except that the areas under the magnesium peak have been normalized by the carbon peak at 247.8 nm and the germanium peak at 265.1 nm, respectively. Because the germanium and carbon peaks are approximately the same size for all samples, normalizing by the C 247.8 nm peak or Ge 265.1 nm peak does not substantially alter the calibration fits; but only slightly improves some fits and worsens others. Normalizing by C 247.8 nm or Ge 265.1 nm does help in assuring that unexpected matrix effects do not substantially alter analytic predictions. Figure 6d presents corresponding LIBS calibration data for the Mg 278.5 nm peak using a gate delay of 3 µs. In Fig. 6e, the results of Fig. 6d have been normalized by the C 247.8nm peak. The plots in Fig. 6 illustrate that gate delays of either 1 or 3 µs can be used to build useful LIBS calibration curves for Mg, and that normalizing by C 247.8 nm or Ge 265.1 nm does not substantially alter any of the calibration fits.

The coefficients of determination (R^2) and the 95% prediction uncertainties ($U_{95\%}$) used to define the 95% confidence intervals for all of the fits in Fig. 6 are listed in Table 2, which also includes the best fit parameters for the Mg 309.1 nm and the Mg 518.4 nm peaks. The R^2 values for the NIST samples are 0.97 or greater for all three Mg peaks for nearly all normalization methods. The calibration fits to the non-NIST samples are slightly poorer; and, interestingly, normalizing the Mg peaks by the C 248 nm peak or the Ge 265 nm peak has a much greater impact on the fits for the non-NIST samples than it does for the NIST samples. Normalizing the Mg peaks by the Ge 265.1 nm peak significantly improves the fits for the non-NIST samples and raises the R^2 values to above 0.90 for all peaks. The fit parameters for the best fits for each peak are shown in bold type in Table 2 and demonstrate that the univariate LIBS model is capable of predicting Mg concentrations of the non-NIST samples with an uncertainty of approximately 100 ppm.

Table 2. Fit parameters for three Mg peaks, including correlation coefficients (R^2) and prediction uncertainties ($U_{95\%}$) for gate delays (GD) of 1 and 3 µs without normalization and also normalized by the C 248 nm and Ge 265 nm peaks. The fit parameters for the best fits are shown in bold type.

		R^2					$U_{95\%}$				
		GD = 1 µs			GD = 3 µs		GD = 1 µs			GD = 3 µs	
Normalization→		None	C248	Ge265	None	C248	None	C248	Ge265	None	C248
Peak (nm) ↓											
NIST SRMs	Mg 278.5	0.99	0.99	0.99	**0.99**	0.99	342	498	469	**277**	413
	Mg 309.1	0.99	0.99	0.98	**0.99**	0.94	347	514	575	**335**	858
	Mg 518.4	0.98	0.97	0.98	**1.00**	0.97	544	719	553	**233**	647
non-NIST samples	Mg 278.5	0.84	0.91	**0.99**	0.84	0.95	344	259	**83**	252	132
	Mg 309.1	0.40	0.43	**0.91**	0.48	0.68	668	650	**234**	450	351
	Mg 518.4	0.86	0.91	**1.00**	0.95	0.99	328	265	**51**	142	61

The areas under the Ca peak at 370.6 nm for all of the NIST and non-NIST samples are plotted in Fig. 7a as a function of Ca concentration for a gate delay (GD) of 1 µs. Following the format established in Fig. 6, standard reference materials (SRMs) from NIST that have certified concentration values are shown as solid dots, and non-NIST samples are shown as hollow circles. The solid and dashed fit lines also have the same representations as in Fig. 6 (the fit lines for NIST SRMs are solid, while the fit lines for the non-NIST samples are dashed). Estimated Ca concentrations for the non-NIST sample were obtained from the estimated values in Fig. 3. In Figures 7b and 7c the areas under the calcium peaks have been normalized by the carbon peak at 247.8 nm and the germanium peak at 265.1 nm, respectively. Figure 7d presents corresponding LIBS calibration data for the Ca 370.6 nm peak using a gate delay of 3 µs. In Fig. 7e, the results of Fig. 7d have been normalized by the C 247.8 nm peak.

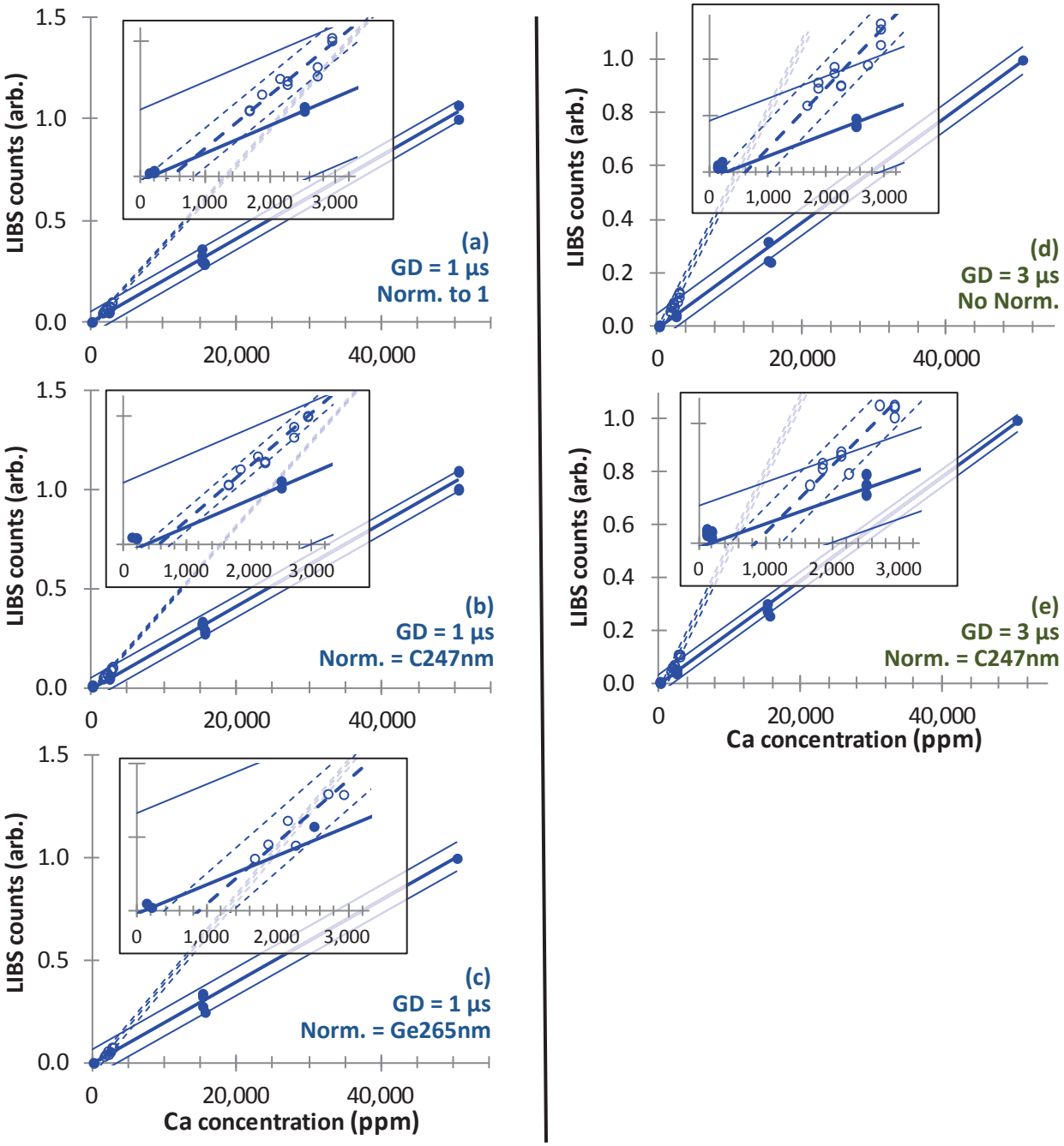

Figure 7. LIBS calibration data for calcium using the Ca II 370.6 nm peak. The area under the peak is plotted as a function estimated Ca concentration for all NIST (solid dots) and non-NIST samples (hollow circles). Ca concentration data was obtained for the NIST and non-NIST samples from Figures 1 and 3, respectively. In (a), the gate delay (GD) was 1 µs and the curves were normalized to have a maximum of unity. Plots (b) and (c) are similar to (a) except that the areas under the Ca 370.6 nm peak has been normalized by the carbon peak at 247.8 nm and the germanium peak at 265.1 nm, respectively. (d) and (e) are similar to (a) and (b), respectively, except that GD = 3 µs.

The calibration curves for calcium are different from the magnesium curves in that the non-NIST samples appear to follow a distinctly different trend than the corresponding fits for the NIST SRMs. A similar phenomenon is also observed for Fe and Mn and may also be present in fits for K, Na, Al, and Si,

as shown in the Appendix in Figures A.1 through A.7. It is not clear why the non-NIST samples for some elements follow a different calibration trend than that of the NIST SRMs. All of the samples were ground to similar fine particles sizes (minus 80 microns) and were subjected to a similar pelletization procedure. The LIBS measurements were randomized with some repeated points (points that have the same ppm values in Fig. 6), and it was verified that equipment drift over the time duration of the experiments was not a significant factor. One possibility is that the measured concentrations of some inorganic elements of the non-NIST samples reported in Figures 3 and 4 are in error. However, consistent data was obtained from three separate methods and instruments at different laboratories, so it is unlikely that the calibration data in Figures 3 and 4 are faulty. Regardless of the reason for the discrepancy, assuming that the calibration data in Figures 3 and 4 is accurate, the LIBS calibration curves for the non-NIST samples are valid. Perhaps the cause of the discrepancy between the NIST SRMs and the non-NIST samples will become clearer as additional samples are tested and validated with independent ICP-OES methods.

The coefficients of determination (R^2) and the 95% prediction uncertainties ($U_{95\%}$) used to define the 95% confidence intervals for all of the fits in Fig. 7 are listed in Table 3, which also includes the best fit parameters for the Ca 849.8 nm and the Ca 315.9 nm peaks. The R^2 values for the NIST samples are all 0.97 or greater for all three Ca peaks for all normalization methods. The calibration fits to the non-NIST samples are slightly poorer; however, normalizing the Ca peaks by the C 248 nm peak or the Ge 265 nm peak improves the fits, resulting in R^2 values as high as 0.96. The fit parameters for the best fits for each peak are shown in bold type in Table 3 and demonstrate that the univariate LIBS model is capable of predicting Ca concentrations of the non-NIST samples with an uncertainty of approximately 100 ppm, similar to that of the calibration curves for Mg. LIBS calibration curves for K, Na, Al, Fe, Mn, P, and Si are available in the Appendix as Figures A.1 – A.7. Tables A.1 – A.7 in the Appendix provide the curve fit parameters for the same elements.

Table 3. Fit parameters for three Ca peaks, including correlation coefficients (R^2) and prediction uncertainties ($U_{95\%}$) for gate delays (GD) of 1 us and 3 µs without normalization and also normalized by the C 248 nm and the Ge 265 nm peaks. The fit parameters for the best fits are shown in bold type.

		R^2					$U_{95\%}$				
		GD = 1 µs			GD = 3 µs		GD = 1 µs			GD = 3 µs	
Normalization→	Peak (nm) ↓	None	C248	Ge265	None	C248	None	C248	Ge265	None	C248
NIST SRMs	Ca 370.6	1.00	0.99	0.99	0.99	**1.00**	1144	1189	1409	1196	**809**
	Ca 849.8	1.00	1.00	0.97	0.99	**1.00**	1012	794	2484	1416	**691**
	Ca 315.9	0.98	0.99	0.98	0.99	**0.99**	2094	1898	2128	1582	**1098**
non-NIST samples	Ca 370.6	0.89	**0.96**	0.84	0.82	0.88	157	**93**	176	191	158
	Ca 849.8	0.72	0.89	**0.90**	0.69	0.83	245	157	**144**	252	184
	Ca 315.9	0.68	**0.90**	0.88	0.28	0.45	265	**150**	154	381	334

The calibration results presented in Tables 1 to 3 and Tables A-1 to A-7 demonstrate that LIBS is a promising rapid screening technique for Al, Ca, Fe, Mg, Mn, P, K, Na and Si. Figure 8 compares the best available LIBS calibration models using gate delays of 1 and 3 µs for the concentrations of Ca, Mg, K, and Na in the six NIST SRMs with the concentrations of those elements determined using the three ICP-OES methods described above. The predicted elemental concentrations are plotted as functions of the NIST certified values and have been normalized by the NIST certified values, such that the diagonal lines represent agreement with the NIST certified values. The dashed vertical lines mark elemental concentrations as certified by NIST. For all of these elements, the LIBS method and all three ICP-OES

methods yielded concentration values in good agreement with the NIST certified values with only a couple of exceptions, demonstrating that the the LIBS method is comparable in accuracy and reliability to the three ICP-OES methods. Considering the uncertainty in the NIST certified values and additional errors due to sample splitting and equipment limitations, it is difficult to determine which method is actually the most accurate. Figure 9 features a similar comparison of the LIBS calibration models using gate delays of 1 and 3 μs for the concentrations of Al, Fe, Mn, and P in the six NIST SRMs with the concentrations of those elements determined using the three ICP-OES methods described above. As noted previously in connection with Fig. 4, the'2 acid' method exhibited results for Al that were significantly different than that of the other two ICP-OES methods for all samples. Other than that, however, the results for all samples and elements are in good agreement, and again, the accuracy and reliability of the LIBS method is comparable to that of the ICP-OES methods.

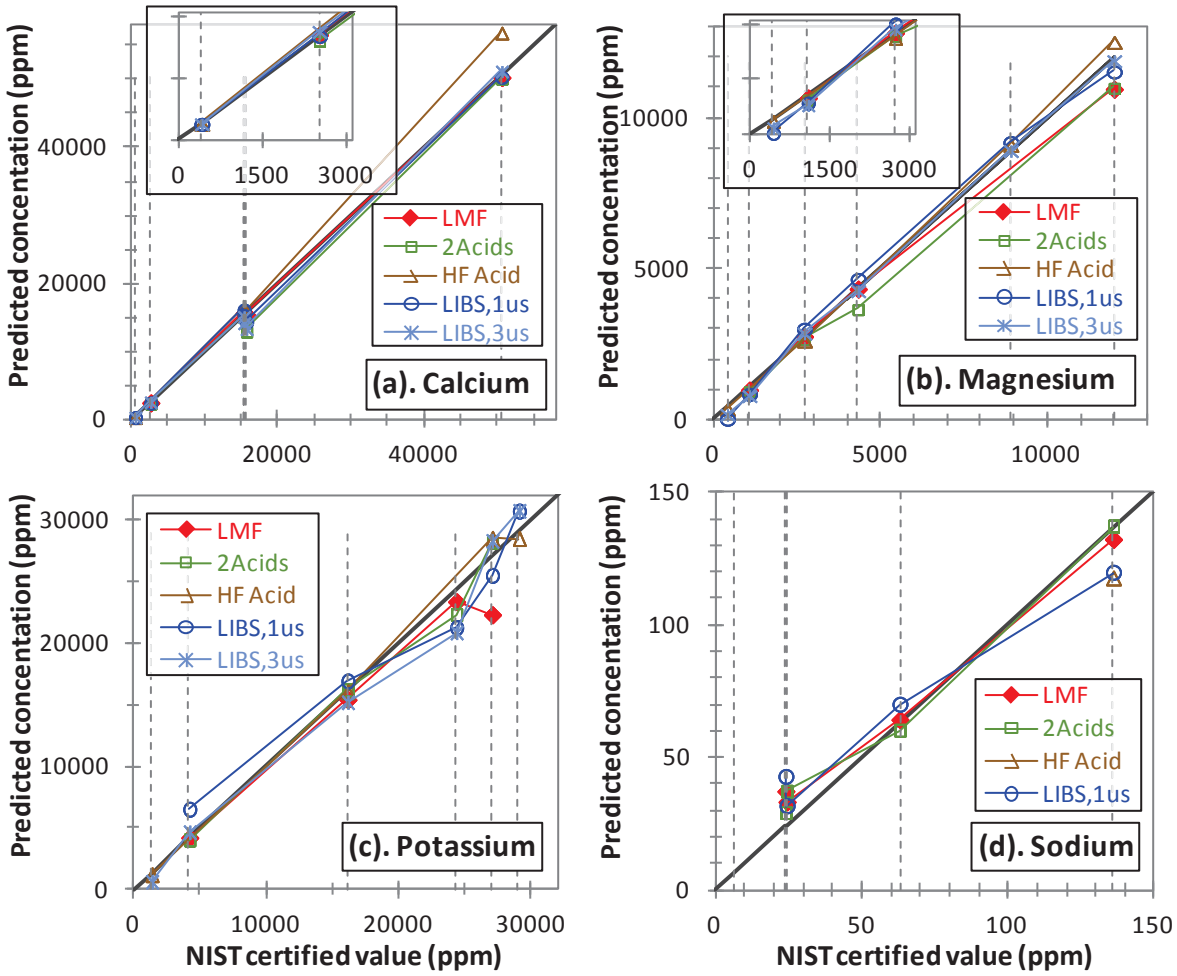

Figure 8. Comparison of concentrations of Ca, Mg, K, and Na of six NIST SRMs predicted using LIBS with GD = 1 and 3 μs with three ICP-OES methods, including HF acid digestion, HNO_3 and $HClO_4$ acid digestions (labeled '2 Acids'), and a lithium metaborate fusion (LMF) method. All values have been normalized by the NIST certified values.

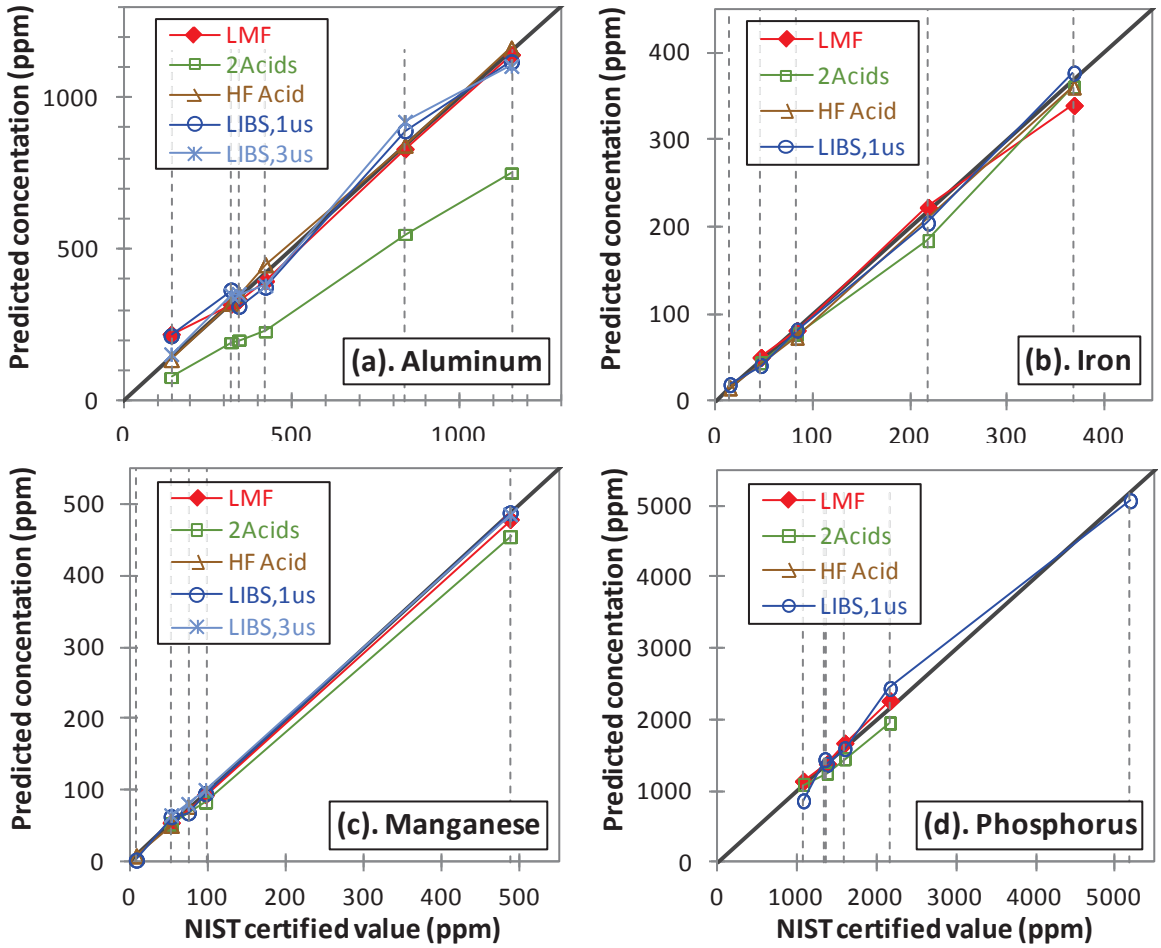

Figure 9: Measured concentrations of Al, Fe, Mn, and P for the same NIST SRMs and using the same methods described in Fig. 8.

Figures 10 and 11 compare LIBS calibrations for the elements of interest with results obtained from the three ICP-OES methods for the six non-NIST samples. The LIBS method yields results that are comparable in accuracy and reliability to the three ICP-OES methods for Ca, Mg, Na, Al, Fe and Si. The LIBS method is somewhat poorer for K, Mn and P. Figure 11f compares results from the LIBS method for Si with that of the three ICP-OES methods for the six NIST SRMs and shows that the LIBS method is less accurate for the NIST SRMs than it is for the non-NIST samples. The fact that the LIBS results for gate delays of 1 and 3 μs are nearly identical indicates that an inadvertent error is not likely the cause of the observed discrepancies. Figure 12 displays the sum of Al, Ca, Fe, Mg, Mn, P, K, Na and Si concentrations (which comprise nearly all of the total ash except Cl and S) for the NIST SRMs and six non-NIST samples featured in Figures 1 through 11 as measured by the lithium metaborate fusion (LMF) method and the predictions by the best LIBS calibrations. The estimated ash concentrations on the x-axis were determined by summing the contributions of the individual elements, using the NIST certified values for the NIST SRMs (Figures 1 and 2) and the estimated values for the non-NIST samples (Figures 3 and 4). It is observed that the LIBS method predicts total ash very well and even better than the LMF method for samples with high potassium content for which the LMF method loses accuracy (see Figures 8 and 10).

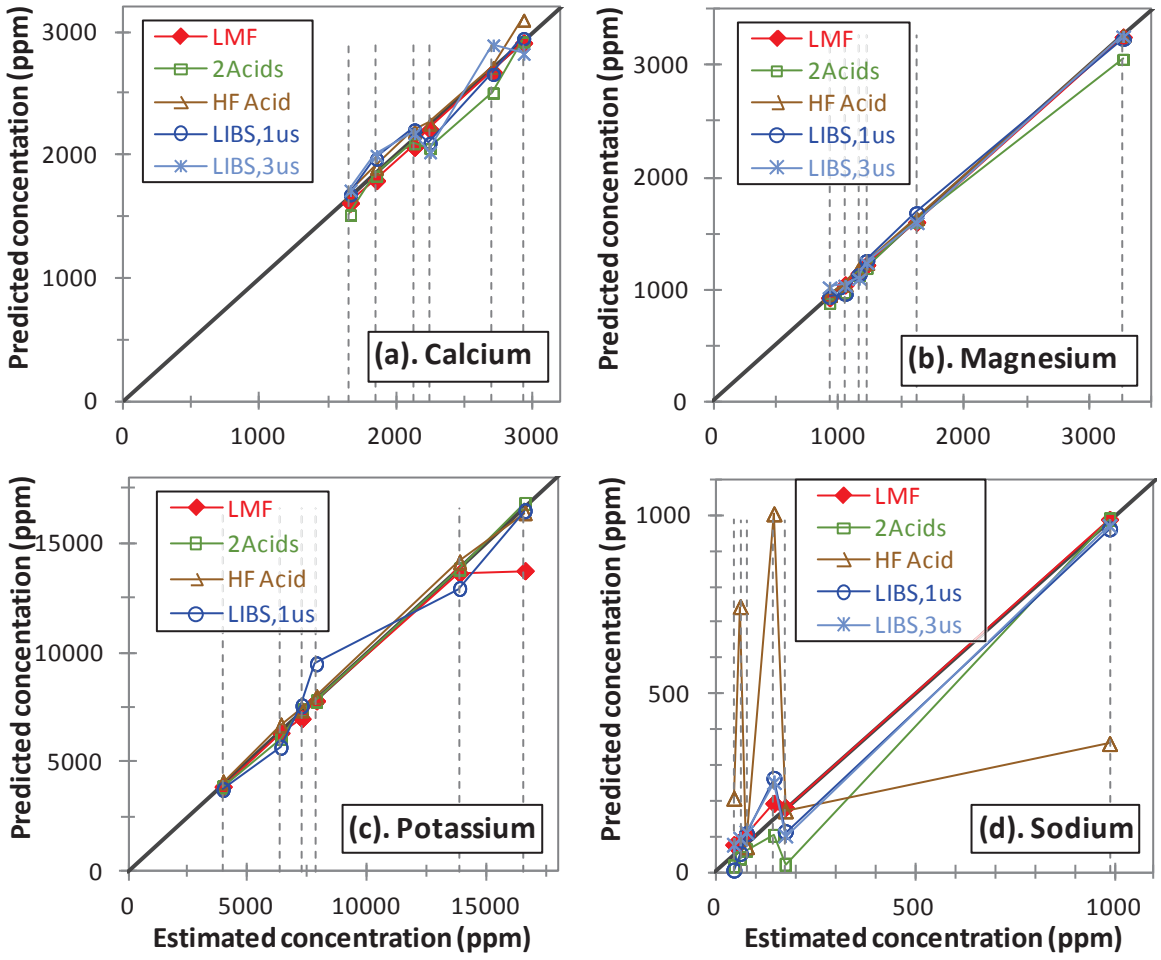

Figure 10. Measured concentrations of Ca, Mg, K, and Na for six non-NIST samples as determined using ICP-OES methods with HF acid digestion, HNO_3 and $HClO_4$ acid digestions (labeled '2 Acids'), and a lithium metaborate fusion (LMF) method. All values have been normalized by the NIST certified value.

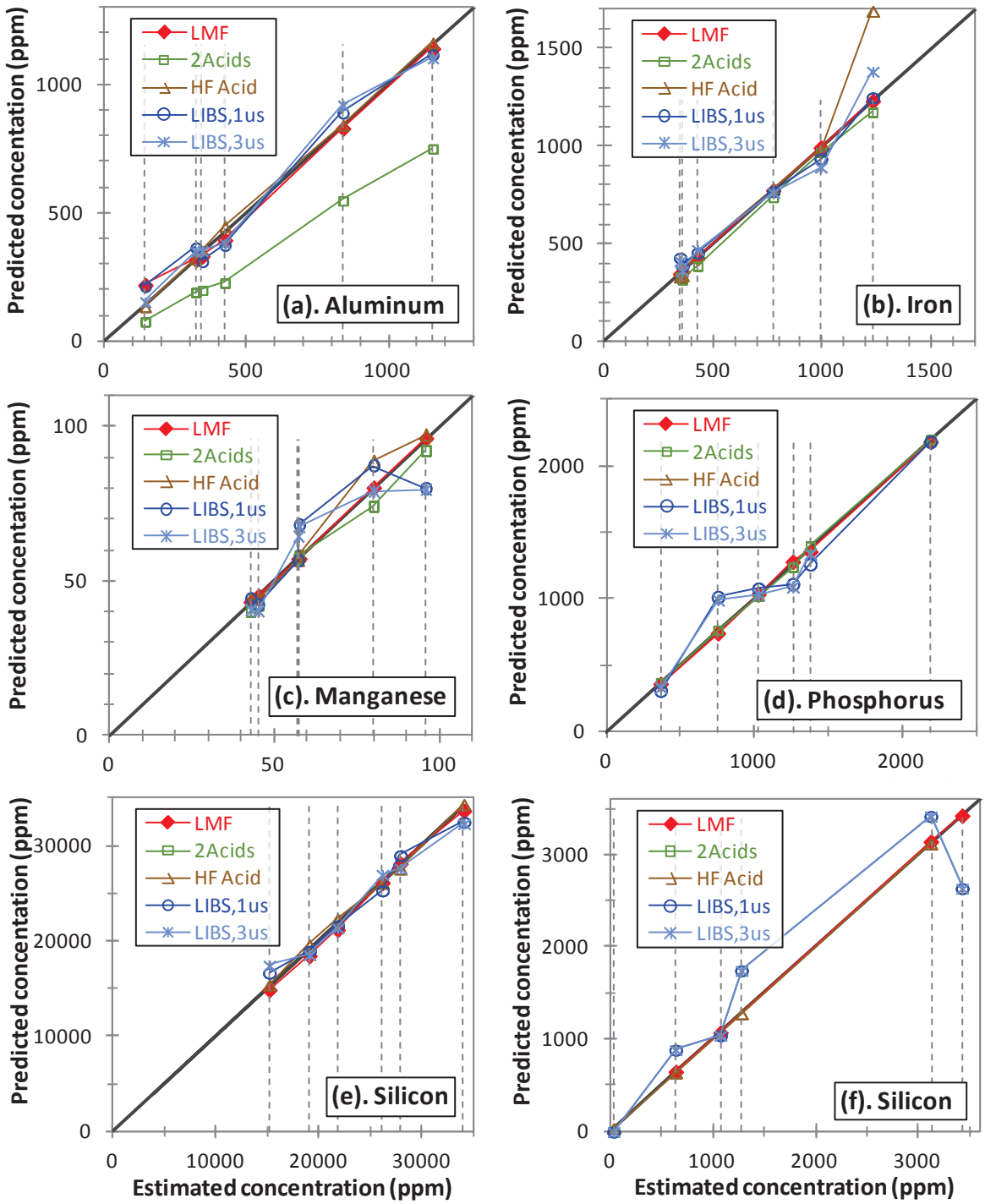

Figure 11. Measured concentrations of Al, Fe, Mn, P and Si for same non-NIST samples and using the same methods described in Fig. 10. (f) contains similar Si concentration data for the NIST SRMs.

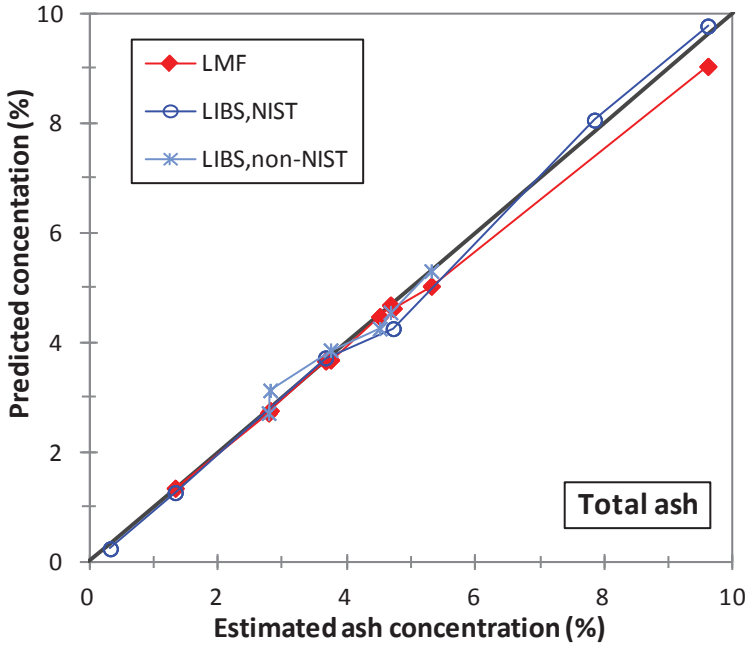

Figure 12. Concentrations of total ash (including Al, Ca, Fe, Mg, Mn, P, K, Na and Si, excluding Cl and S) for the NIST SRMs and six non-NIST samples featured in Figures 1 through 11 as predicted by the lithium metaborate fusion (LMF) method and the best LIBS calibration curve for each constituent species. Estimated ash concentrations were determined by summing the contributions of the individual elements, using the NIST certified values for the NIST SRMs (Figures 1 and 2) and the estimated values for the non-NIST samples (Figures 3 and 4).

5. CONCLUSIONS AND SUMMARY

The results from the LIBS calibrations for Al, Ca, Fe, Mg, Mn, P, K, Na and Si has been presented in Table 1 and Figures 8 through 11 and indicate that LIBS is promising as a rapid screening technique with an accuracy comparable to that of the acid digestion methods for all of the elements. Importantly, the LMF and acid digestion methods have benefited from many years of widespread research and repeated use, while the LIBS approach is yet emerging for measuring inorganic constituents in biomass. Accordingly, significant improvement is expected in the LIBS approach. For example, the LIBS calibrations in this work employ univariate curve fits, which are usually quite poor compared multivariate calibrations, although the simplicity of univariate methods makes them attractive. A further consideration is that the univariate LIBS calibrations exhibit a high degree of correlation, considering uncertainties in calibration data, and it is possible that multivariate models would only improve the fits by modeling experimental noise, which could make the fits less reliable for new samples. Multivariate models do have advantages, though, in being able to account for interaction effects between elements of interest. It has also been demonstrated in Fig. 12 that LIBS is useful for measuring total ash content minus, except Cl and S. Further refinement to the LIBS technique, such as a more sensitive detector or the use of an argon purge gas should make it possible to reliably analyze Cl, S and possibly O, N, and H.

It was observed that the LIBS calibration curves for some elements for non-NIST samples followed different trends than the corresponding fits for the NIST SRMs. The reason for this discrepancy is not clear. All of the samples were ground to similar fine particles sizes (minus 80 microns) and were subjected to a similar pelletization procedure. The LIBS measurements were randomized with some repeated points, and it was verified that equipment drift over the time duration of the experiments was not

a significant factor. It is also unlikely that the calibration data for the non-NIST samples are in error because similar results were obtained using three separate methods and instruments at different laboratories. Regardless of the reason for the discrepancy, assuming that the calibration data is accurate, the LIBS calibration curves for the non-NIST samples are valid. Perhaps the cause of the discrepancy between the NIST SRMs and the non-NIST samples will become clearer as additional samples are tested and validated with independent ICP-OES methods.

6. REFERENCES

Alvarado, J.S., T. J. Neal, L. L. Smith and M. D. Erickson, "Microwave dissolution of plant tissue and the subsequent determination of trace lanthanide and actinide elements by inductively coupled plasma-mass spectrometry," *Anal. Chim. Acta*, 322(1-2), 11–20 (1996).

Araujo, G.C.L., M.H. Gonzalez, A.G. Ferreira, A.R. . Nogueira, J.A. Nobrega, "Effect of acid concentration on closed-vessel microwave-assisted digestion of plant materials," Spectrochim. Acta, Part B 57, 2121–2132 (2002,).

Baker, J.H. and T. Grewelin, "Extraction procedure for quantitative determination of six elements in plant tissue," J. Agric. Food Chem. 15(2), 340-344 (1967).

Bevington, P.R. and D.K. Robinson, Data reduction and error analysis for the physical sciences, McGraw Hill Publishing, NY, NY (2003). Pg. 61.

Braga, J.W.B., L. C. Trevizan, L. C. Nunes, I. A. Rufini, D. S. Junior and F. J. Krug, "Comparison of univariate and multivariate calibration for the determination of micronutrients in pellets of plant materials by laser induced breakdown spectroscopy," Spectrochim. Acta, Part B, 65, 66–74 (2010).

Draper, N.R., and H.S. Smith, "Applied Regression Analysis," John Wiley & Sons, Inc. Danvers, MA (1998).

Gornushkin, S.I., I.B. Gornushkin, J.M. Anzano, B.W. Smith, J.D. Winefordner, "Effective normalization technique for correction of matrix effects in laser-induced breakdown spectroscopy detection of magnesium in powdered samples," Appl. Spectrosc. 56, 433–436 (2002).

Labbe, N., I.M. Swamidoss, N. Andre, et. al., "Extraction of information from laser-induced breakdown spectroscopy spectral data by multivariate analysis", Applied Optics 47(31), G158-G165 (2008).

Momen, A., G.A. Zachariadis, A.N. Anthemidis and J.A. Stratis, "Investigation of four digestion procedures for multi-element determination of toxiz and nutrient elements in legumes by inductively coupled plasma-optical emission spectroscopy," Anal. Chim. Acta, 565, 81–88 (2006).

Nunes, L.C., J.W.B. Braga, L. . Trevizan, P.F. de Souza, G.G. de Carvalho, D. Santos Jun., R.J. Poppie, F.J. Krug, "Effective normalization technique for correction of matrix effects in laser-induced breakdown spectroscopy detection of magnesium in powdered samples," Appl. Spectrosc. 56, 433–436 (2002).

Sun, Q., M. Tran, B.W. Smith, J.D. Winefordner, "Direct determination of P, Al, Ca, Cu, Mn, Zn, Mg and Fe in plant materials by laser-induced plasma spectroscopy," Canadian J. Anal. Sci. Spectrosc. 44, 164–170 (1999).

APPENDIX A. LIBS CALIBRATION DATA BY ELEMENT

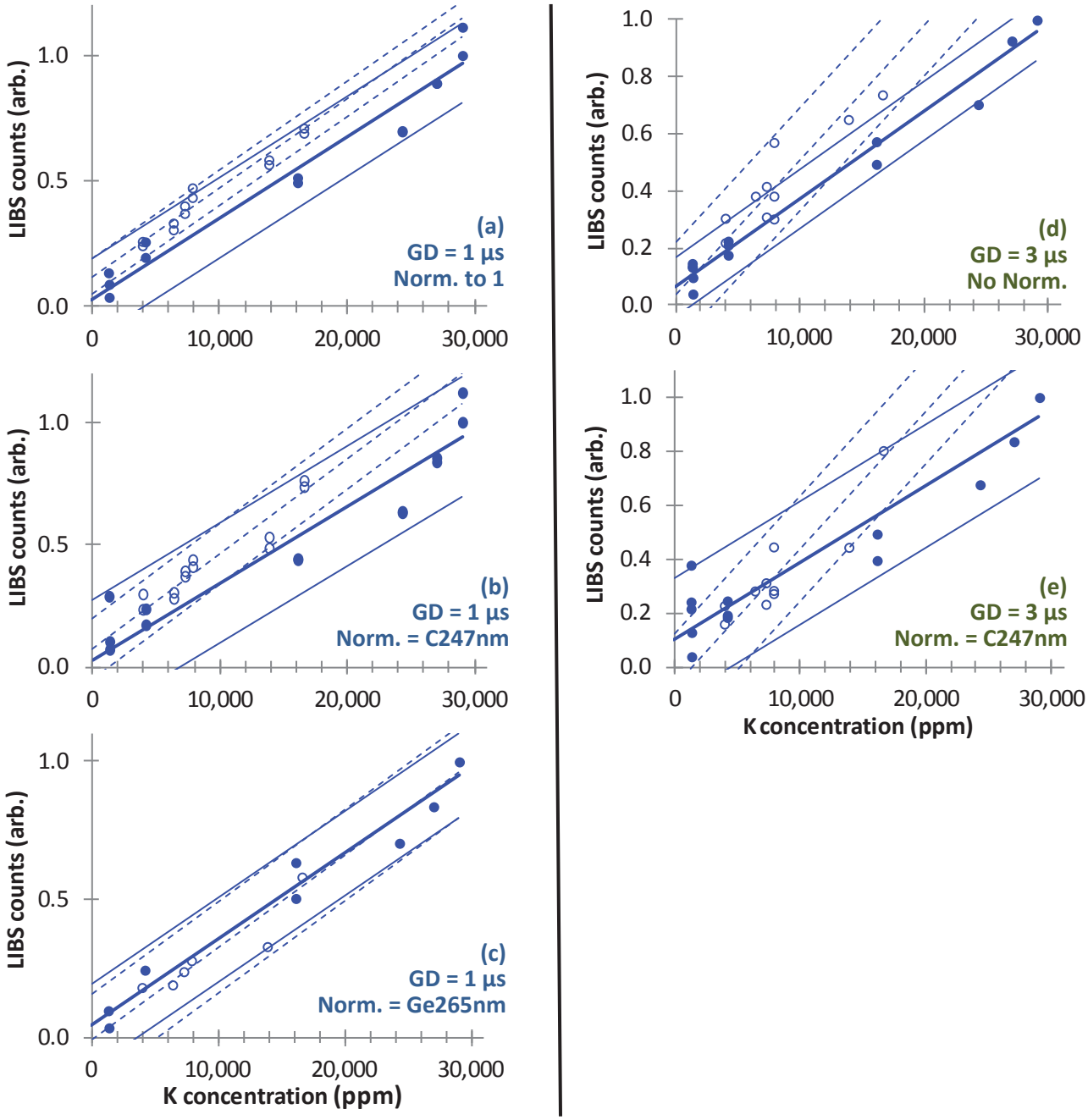

Figure A.1: LIBS calibration data for potassium using the K 766.4 nm peak. The area under the peak is plotted as a function estimated K concentration for all NIST (solid dots) and non-NIST samples (hollow circles). K concentration data was obtained for the NIST and non-NIST samples from Figures 1 and 3, respectively. In (a), the gate delay (GD) was 1 µs and the curves were normalized to have a maximum of unity. Plots (b) and (c) are similar to (a) except that the areas under the K 766.4 nm peak has been normalized by the carbon peak at 247.8 nm and the germanium peak at 265.1 nm, respectively. (d) and (e) are similar to (a) and (b), respectively, except that GD = 3 µs.

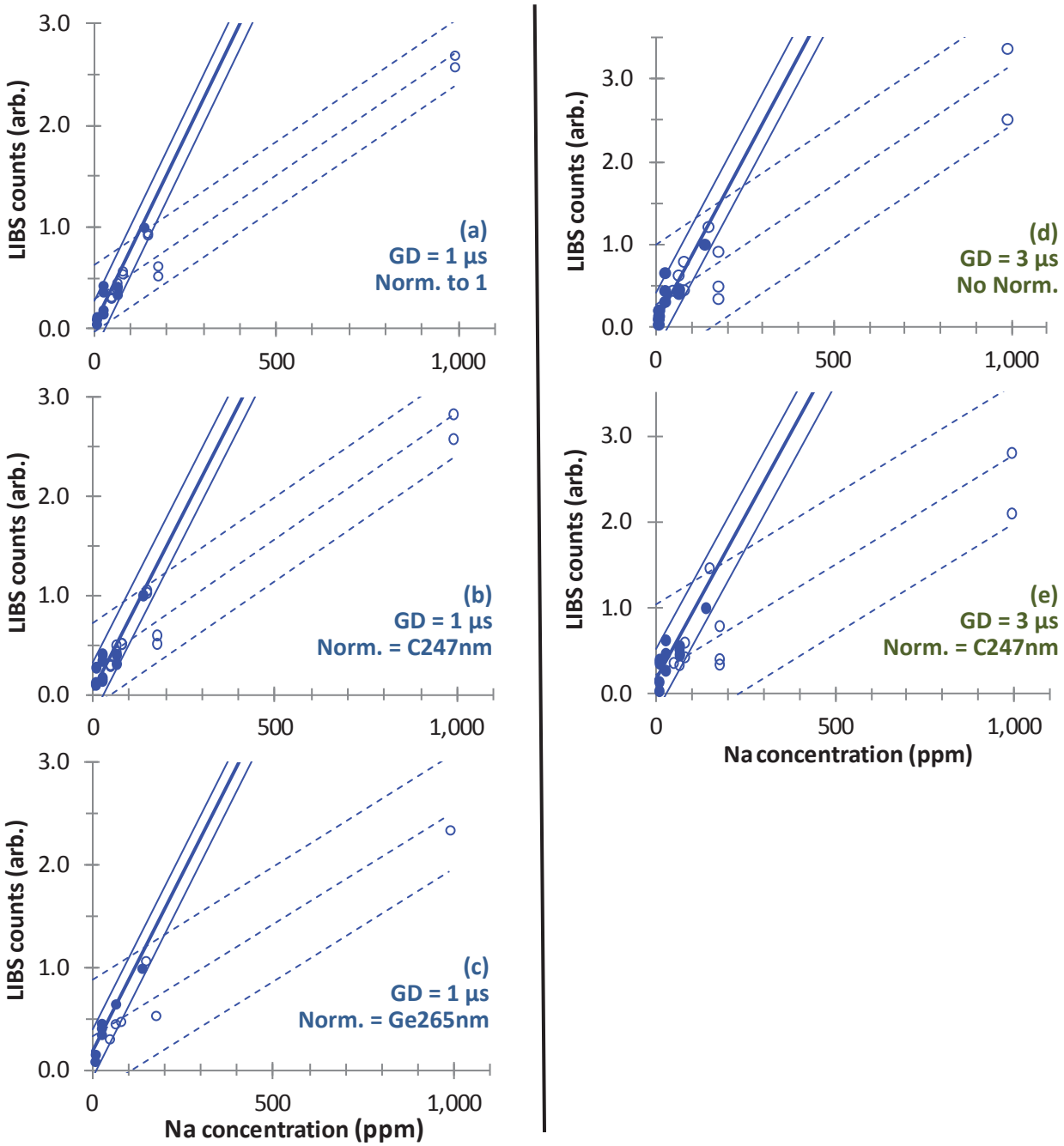

Figure A.2: LIBS calibration data for potassium using the Na 588.9 nm peak. The area under the peak is plotted as a function estimated Na concentration for all NIST (solid dots) and non-NIST samples (hollow circles). Na concentration data was obtained for the NIST and non-NIST samples from Figures 1 and 3, respectively. In (a), the gate delay (GD) was 1 µs and the curves were normalized to have a maximum of unity. Plots (b) and (c) are similar to (a) except that the areas under the Na 588.9 nm peak has been normalized by the carbon peak at 247.8 nm and the germanium peak at 265.1 nm, respectively. (d) and (e) are similar to (a) and (b), respectively, except that GD = 3 µs.

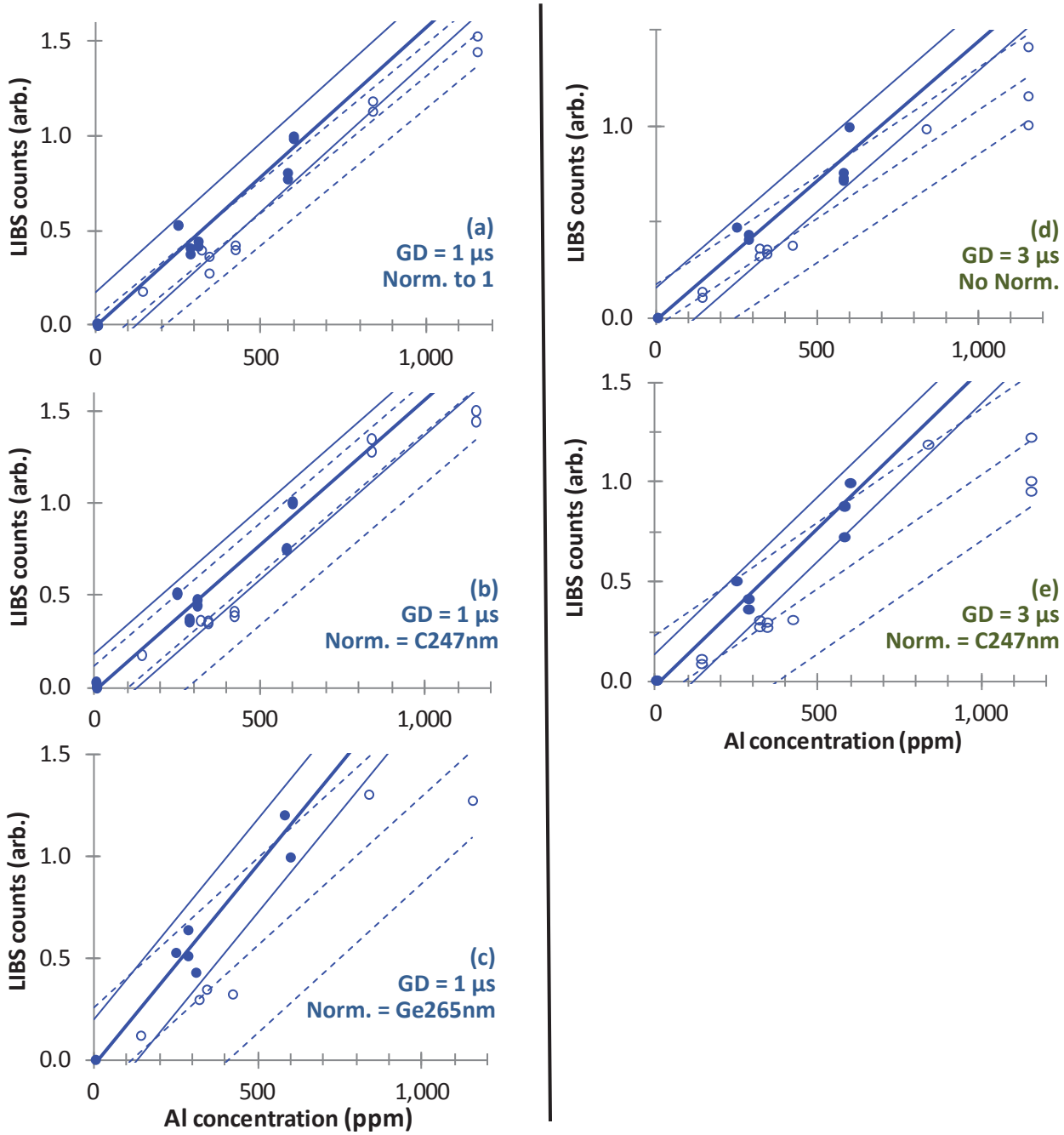

Figure A.3: LIBS calibration data for aluminum using the Al 308.2 nm peak. The area under the peak is plotted as a function estimated Al concentration for all NIST (solid dots) and non-NIST samples (hollow circles). Al concentration data was obtained for the NIST and non-NIST samples from Figures 2 and 4, respectively. In (a), the gate delay (GD) was 1 µs and the curves were normalized to have a maximum of unity. Plots (b) and (c) are similar to (a) except that the areas under the Al 308.2 nm peak has been normalized by the carbon peak at 247.8 nm and the germanium peak at 265.1 nm, respectively. (d) and (e) are similar to (a) and (b), respectively, except that GD = 3 µs.

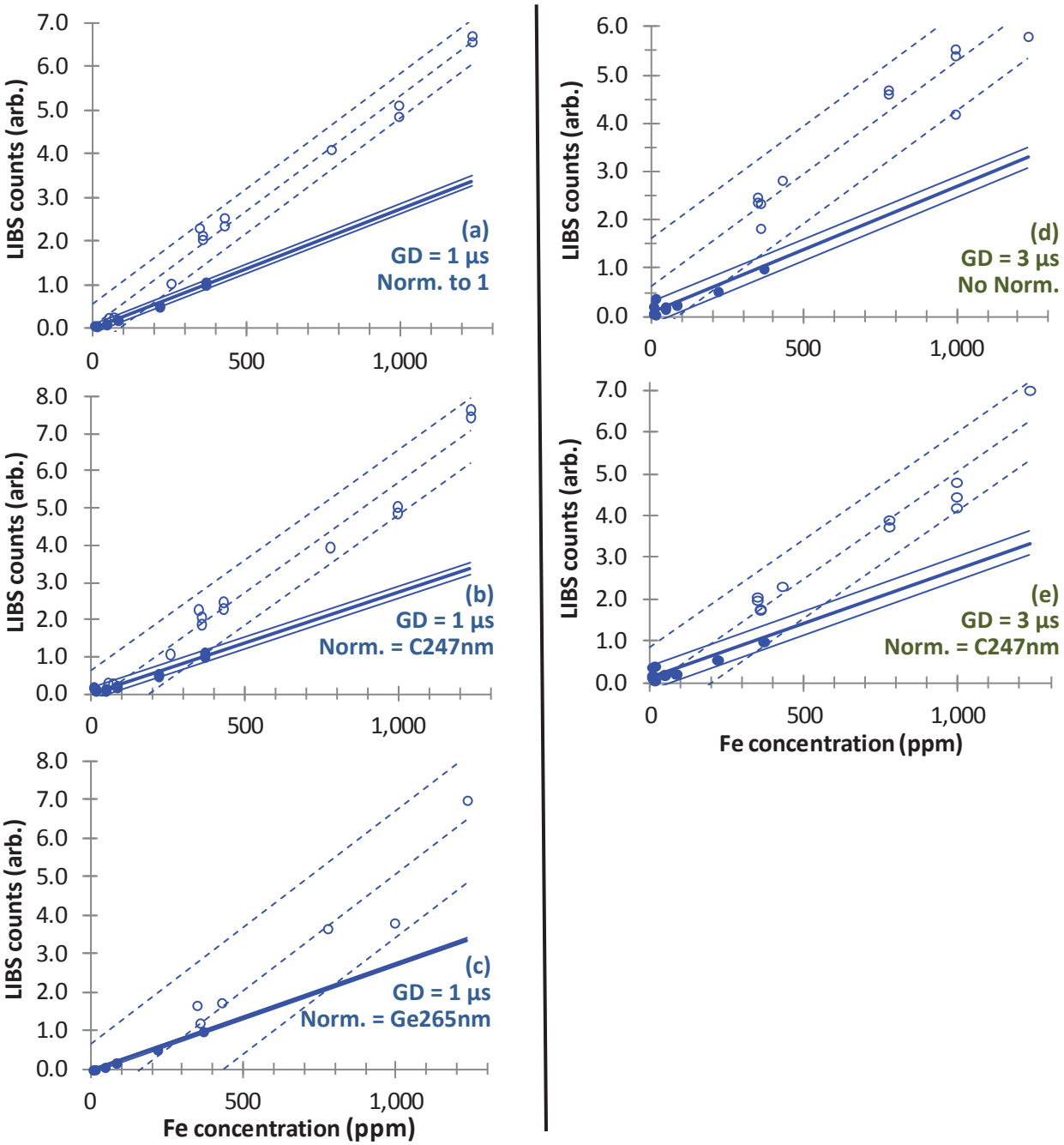

Figure A.4: LIBS calibration data for iron using the Fe 259.9 nm peak. The area under the peak is plotted as a function estimated Fe concentration for all NIST (solid dots) and non-NIST samples (hollow circles). Fe concentration data was obtained for the NIST and non-NIST samples from Figures 2 and 4, respectively. In (a), the gate delay (GD) was 1 µs and the curves were normalized to have a maximum of unity. Plots (b) and (c) are similar to (a) except that the areas under the Fe 259.9 nm peak has been normalized by the carbon peak at 247.8 nm and the germanium peak at 265.1 nm, respectively. (d) and (e) are similar to (a) and (b), respectively, except that GD = 3 µs.

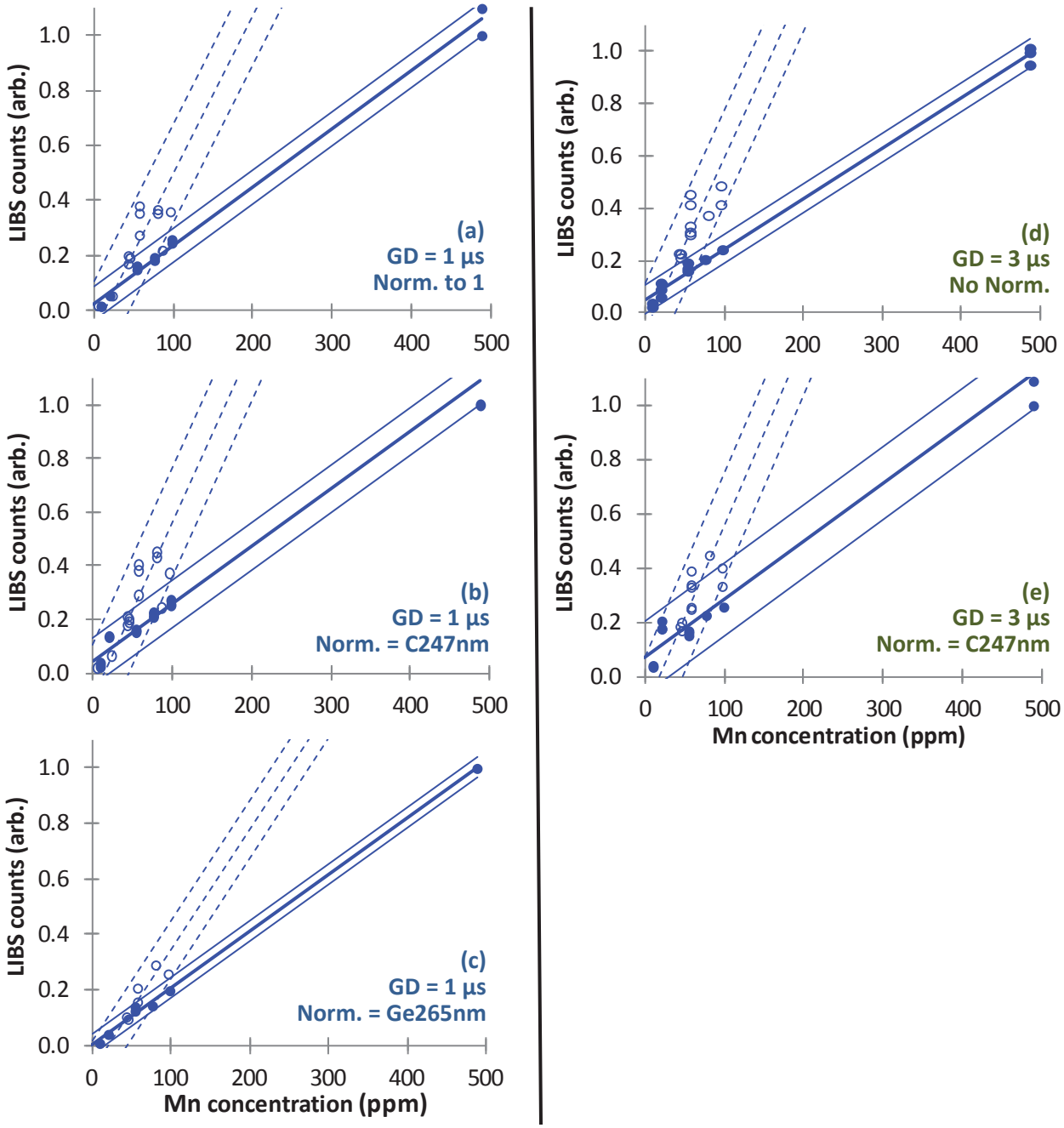

Figure A.5: LIBS calibration data for manganese using the Mn 257.6 nm peak. The area under the peak is plotted as a function estimated Mn concentration for all NIST (solid dots) and non-NIST samples (hollow circles). Mn concentration data was obtained for the NIST and non-NIST samples from Figures 2 and 4, respectively. In (a), the gate delay (GD) was 1 µs and the curves were normalized to have a maximum of unity. Plots (b) and (c) are similar to (a) except that the areas under the Mn 257.6 nm peak has been normalized by the carbon peak at 247.8 nm and the germanium peak at 265.1 nm, respectively. (d) and (e) are similar to (a) and (b), respectively, except that GD = 3 µs.

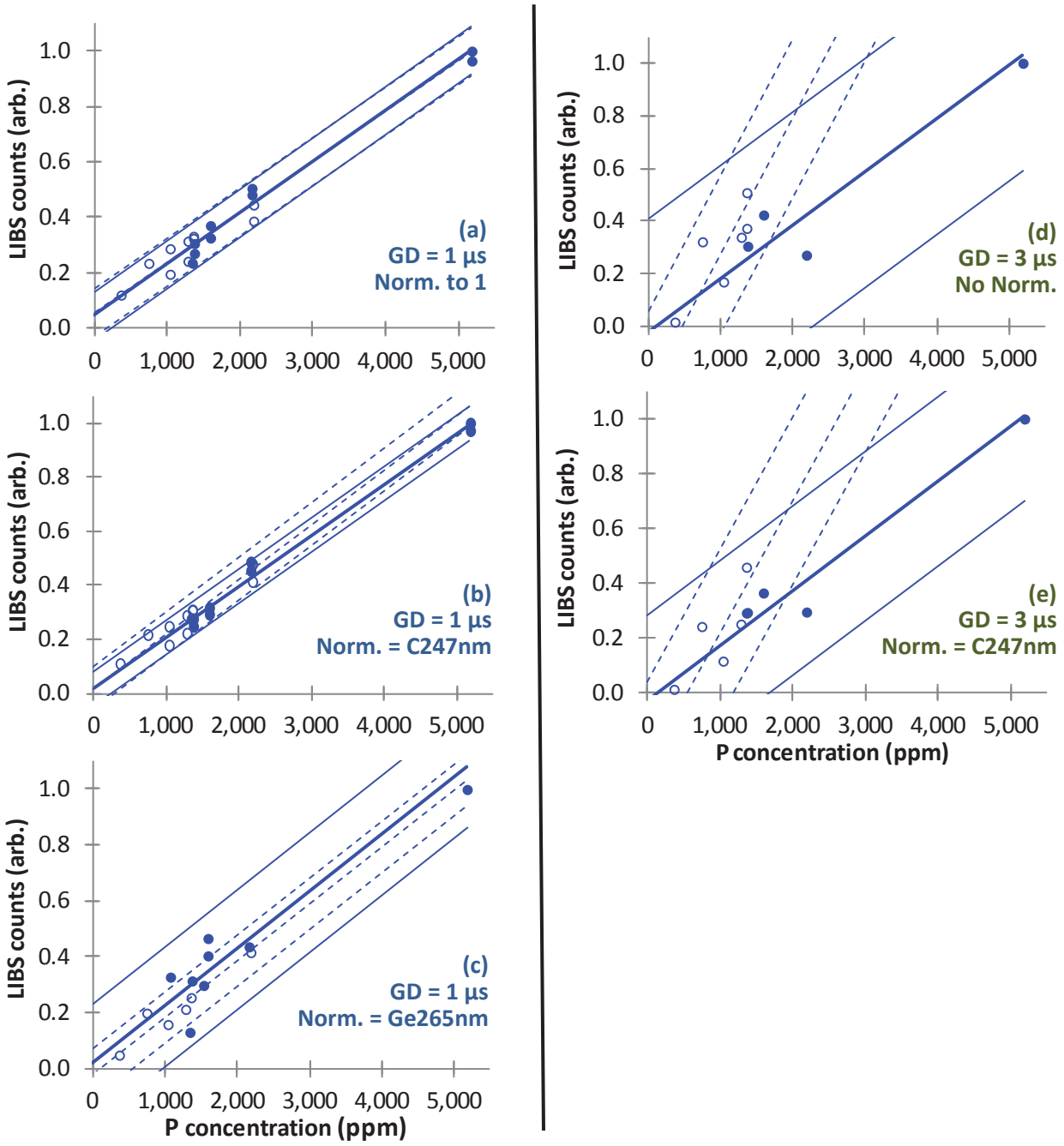

Figure A.6: LIBS calibration data for phosphorus using the P 213.6 nm peak. The area under the peak is plotted as a function estimated P concentration for all NIST (solid dots) and non-NIST samples (hollow circles). P concentration data was obtained for the NIST and non-NIST samples from Figures 2 and 4, respectively. In (a), the gate delay (GD) was 1 µs and the curves were normalized to have a maximum of unity. Plots (b) and (c) are similar to (a) except that the areas under the P 213.6 nm peak has been normalized by the carbon peak at 247.8 nm and the germanium peak at 265.1 nm, respectively. (d) and (e) are similar to (a) and (b), respectively, except that GD = 3 µs.

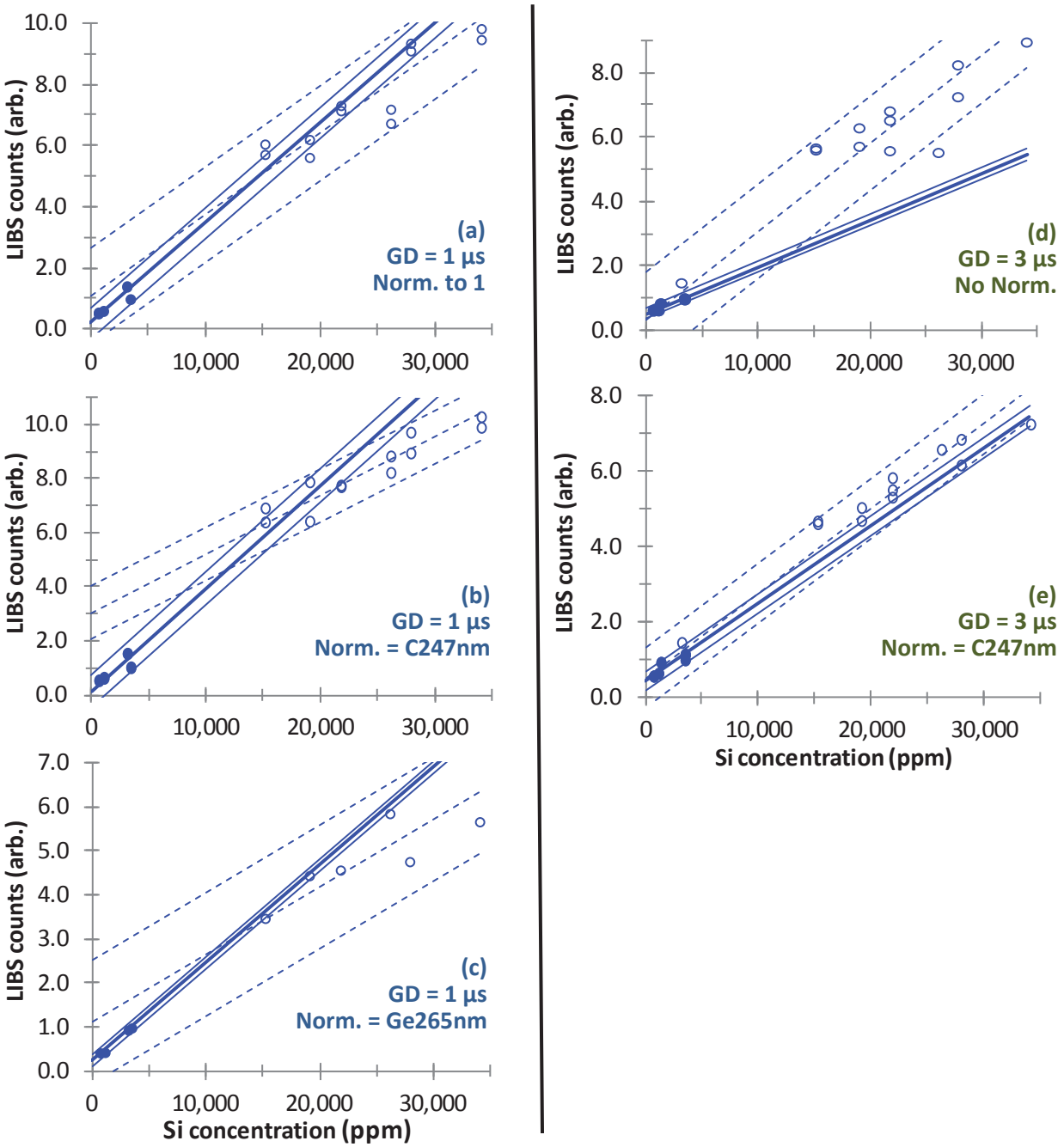

Figure A.7: LIBS calibration data for silicon using the Si 251.6 nm peak. The area under the peak is plotted as a function estimated Si concentration for all NIST (solid dots) and non-NIST samples (hollow circles). Si concentration data was obtained for the NIST and non-NIST samples from Figure 4. In (a), the gate delay (GD) was 1 µs and the curves were normalized to have a maximum of unity. Plots (b) and (c) are similar to (a) except that the areas under the Si 251.6 nm peak has been normalized by the carbon peak at 247.8 nm and the germanium peak at 265.1 nm, respectively. (d) and (e) are similar to (a) and (b), respectively, except that GD = 3 µs.

Table A-1. Fit parameters for three K peaks, including correlation coefficients (R^2) and prediction uncertainties ($U_{95\%}$) for gate delays (GD) of 1 us and 3 µs without normalization and also normalized by the C 248 nm and the Ge 265 nm peaks. The fit parameters for the best fits are shown in bold type.

		R^2					$U_{95\%}$				
		GD = 1 µs			GD = 3 µs		GD = 1 µs			GD = 3 µs	
Normalization→		None	C248	Ge265	None	C248	None	C248	Ge265	None	C248
Peak (nm) ↓											
NIST SRMs	K 766.5	0.96	0.90	0.96	**0.98**	0.88	2260	3554	2014	**1488**	3735
	K 693.9	0.88	0.84	0.90	**0.92**	0.88	3934	4488	3376	**3034**	3676
	K 404.5	0.93	0.89	**0.94**	0.93	0.89	3059	3676	**2525**	2934	3553
non-NIST samples	K 766.5	**0.96**	0.89	0.84	0.91	0.85	**912**	1444	1770	1210	1534
	K 693.9	0.91	0.86	0.86	**0.93**	0.81	1304	1660	1659	**1088**	1726
	K 404.5	0.77	0.73	0.67	**0.76**	0.68	2146	2280	2561	**1954**	2272

Table A-2. Fit parameters for two Na peaks, including correlation coefficients (R^2) and prediction uncertainties ($U_{95\%}$) for gate delays (GD) of 1 us and 3 µs without normalization and also normalized by the C 248 nm and the Ge 265 nm peaks. The fit parameters for the best fits are shown in bold type.

		R^2					$U_{95\%}$				
		GD = 1 µs			GD = 3 µs		GD = 1 µs			GD = 3 µs	
Normalization→		None	C248	Ge265	None	C248	None	C248	Ge265	None	C248
Peak (nm) ↓											
NIST SRMs	Na 589	0.86	0.82	**0.91**	0.73	0.67	14	16	**13**	19	22
	Na 819.5	0.71	**0.81**	0.39	0.71	0.77	21	**17**	33	20	18
non-NIST samples	Na 589	**0.97**	0.95	0.92	0.90	0.83	**60**	75	92	110	140
	Na 819.5	0.52	0.36	0.92	**0.96**	0.94	232	268	92	**68**	85

Table A-3. Fit parameters for three Al peaks, including correlation coefficients (R^2) and prediction uncertainties ($U_{95\%}$) for gate delays (GD) of 1 us and 3 µs without normalization and also normalized by the C 248 nm and the Ge 265 nm peaks. The fit parameters for the best fits are shown in bold type.

		R^2					$U_{95\%}$				
		GD = 1 µs			GD = 3 µs		GD = 1 µs			GD = 3 µs	
Normalization→		None	C248	Ge265	None	C248	None	C248	Ge265	None	C248
Peak (nm) ↓											
NIST SRMs	Al 308.3	0.94	0.93	0.95	0.96	**0.97**	52	56	48	51	**45**
	Al 396.2	0.84	0.87	0.70	**0.98**	0.95	86	77	114	**37**	54
	Al 394.5	0.75	0.78	0.55	**0.97**	0.94	107	100	138	**42**	64
non-NIST samples	Al 308.3	**0.98**	0.95	0.91	0.95	0.89	**51**	78	106	88	128
	Al 396.2	0.90	0.88	0.95	**0.98**	0.97	112	119	80	**49**	72
	Al 394.5	0.91	0.89	0.94	**0.98**	0.96	106	116	82	**54**	76

Table A-4. Fit parameters for three Fe peaks, including correlation coefficients (R^2) and prediction uncertainties ($U_{95\%}$) for gate delays (GD) of 1 us and 3 µs without normalization and also normalized by the C 248 nm and the Ge 265 nm peaks. The fit parameters for the best fits are shown in bold type.

		R^2					$U_{95\%}$				
		GD = 1 µs			GD = 3 µs		GD = 1 µs			GD = 3 µs	
	Normalization→	None	C248	Ge265	None	C248	None	C248	Ge265	None	C248
	Peak (nm) ↓										
NIST SRMs	Fe 259.9	0.98	0.96	**1.00**	0.87	0.79	17	27	**8**	37	48
	Fe 438.3	**0.98**	0.97	0.97	0.96	0.90	**18**	23	21	20	33
	Fe 261.2	**0.97**	0.95	0.92	0.90	0.72	**24**	29	34	33	55
non-NIST samples	Fe 259.9	**0.99**	0.97	0.92	0.91	0.94	**44**	66	98	96	81
	Fe 438.3	**0.96**	0.92	0.86	0.86	0.75	**83**	115	129	118	160
	Fe 261.2	**0.99**	0.97	0.91	0.89	0.91	**46**	73	104	103	94

Table A-5. Fit parameters for two Mn peaks, including correlation coefficients (R^2) and prediction uncertainties ($U_{95\%}$) for gate delays (GD) of 1 us and 3 µs without normalization and also normalized by the C 248 nm and the Ge 265 nm peaks. The fit parameters for the best fits are shown in bold type.

		R^2					$U_{95\%}$				
		GD = 1 µs			GD = 3 µs		GD = 1 µs			GD = 3 µs	
Normalization→		None	C248	Ge265	None	C248	None	C248	Ge265	None	C248
Peak (nm) ↓											
NIST SRMs	Mn 257.6	0.99	0.99	**1.00**	1.00	0.98	13	18	**7**	13	28
	Mn 403.2	0.99	0.98	**1.00**	0.99	0.97	19	23	**7**	15	32
non-NIST samples	Mn 257.6	0.67	0.67	**0.80**	0.57	0.52	14	14	**9**	12	13
	Mn 403.2	0.77	0.74	**0.74**	0.69	0.50	12	12	**10**	10	13

Table A-6. Fit parameters for two P peaks, including correlation coefficients (R^2) and prediction uncertainties ($U_{95\%}$) for gate delays (GD) of 1 us and 3 µs without normalization and also normalized by the C 248 nm and the Ge 265 nm peaks. The fit parameters for the best fits are shown in bold type.

		R^2					$U_{95\%}$				
		GD = 1 µs			GD = 3 µs		GD = 1 µs			GD = 3 µs	
Normalization→		None	C248	Ge265	None	C248	None	C248	Ge265	None	C248
Peak (nm) ↓											
NIST SRMs	P 213.6	0.98	**0.99**	0.88	0.81	0.86	214	**170**	428	492	424
	P 255.3	0.95	**0.96**	0.89	0.87	0.84	314	**287**	408	407	452
non-NIST samples	P 213.6	0.85	0.90	**0.92**	0.67	0.61	211	169	**162**	215	235
	P 255.3	0.77	0.87	**0.94**	0.63	0.68	260	191	**139**	228	212

Table A-7. Fit parameters for three Si peaks, including correlation coefficients (R^2) and prediction uncertainties ($U_{95\%}$) for gate delays (GD) of 1 us and 3 µs without normalization and also normalized by the C 248 nm and the Ge 265 nm peaks. The fit parameters for the best fits are shown in bold type.

		R^2					$U_{95\%}$				
		GD = 1 µs			GD = 3 µs		GD = 1 µs			GD = 3 µs	
Normalization→		None	C248	Ge265	None	C248	None	C248	Ge265	None	C248
Peak (nm) ↓											
NIST SRMs	Si 251.6	**0.75**	0.69	0.20	0.67	0.78	**604**	670	1146	766	624
	Si 243.6	**0.80**	0.74	0.19	0.70	0.76	**544**	623	1155	732	656
	Si 288.2	**0.87**	0.82	0.20	0.79	0.87	**441**	520	1143	616	489
non-NIST samples	Si 251.6	0.82	0.89	0.71	0.95	**0.98**	2616	2047	3314	2563	**1702**
	Si 243.6	0.67	0.67	0.75	0.96	**0.99**	3523	3534	3080	2167	**1268**
	Si 288.2	0.78	0.89	0.84	0.95	**0.98**	2917	2086	2461	2501	**1368**